ACS APPLIED MATERIALS & INTERFACES

www.acsami.org

Research Article

Silk Fibroin-Coated Nano-MOFs Enhance the Thermal Stability and Immunogenicity of HBsAg

Jiabin Zhang,[‖] Kai Wang,[‖] Shiyao Xu, Linlin Chen, Haiquan Gu, Yujie Yang, Qi Zhao, Yurou Huo, Bo Li, Yufei Wang, Yubiao Xie, Nan Li, Jiali Zhang,* Jianxu Zhang,* and Qianxue Li*

Cite This: https://doi.org/10.1021/acsami.3c16358

Read Online

ACCESS | Metrics & More | Article Recommendations | Supporting Information

ABSTRACT: Vaccines are widely regarded as one of the most effective weapons in the fight against infectious diseases. Currently, vaccines must be stored and transported at low temperatures as high temperatures can lead to a loss of vaccine conformation and reduced therapeutic efficacy. Metal−organic frameworks (MOFs), such as zeolitic imidazole framework-8 (ZIF-8), are a new class of hybrid materials with large specific surface areas, high loading rates, and good biocompatibility and are successful systems for vaccine delivery and protection. Silk fibroin (SF) has a good biocompatibility and thermal stability. In this study, the hepatitis B surface antigen (HBsAg) was successfully encapsulated in ZIF-8 to form HBsAg@ZIF-8 (HZ) using a one-step shake and one-pot shake method. Subsequently, the SF coating modifies HZ through hydrophobic interactions to form HBsAg/SF@ZIF-8 (HSZ), which enhanced the thermal stability and immunogenicity of HBsAg. Compared to free HBsAg, HZ and HSZ improved the thermostability of HBsAg, promoted the antigen uptake and lysosomal escape, stimulated dendritic cell maturation and cytokine secretion, formed an antigen reservoir to promote antibody production, and activated $CD4^+$ T and $CD8^+$ T cells to enhance memory T-cell production. Importantly, HSZ induced a strong immune response even after 14 days of storage at 25 °C. Furthermore, the nanoparticles prepared by the one-step shake method exhibited superior properties compared to those prepared by the one-pot shake method. This study highlights the importance of SF-coated ZIF-8, which holds promise for investigating thermostable vaccines and breaking the vaccine cold chain.

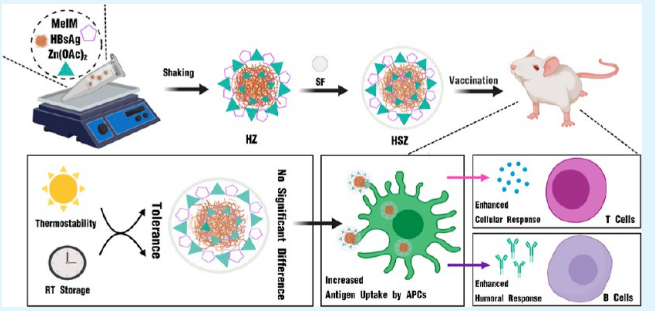

KEYWORDS: *metal−organic frameworks, hepatitis B surface antigen, silk fibroin, vaccine cold chain, thermostability, cellular immunity*

INTRODUCTION

Hepatitis B is a disease that results from infection with the hepatitis B virus (HBV). This viral pathogen is more transmissible than the human immunodeficiency virus, probably due to its ability to survive in the environment for more than 7 days or longer.[1,2] According to statistics, 296 million people worldwide were hepatitis B surface antigen (HBsAg)-positive in 2019, and hepatitis B infection causes more than 800,000 deaths each year, which is more than the number of deaths caused by malaria.[3,4] In China, hepatitis B is highly prevalent and considered endemic, with approximately 130 million people being HBV carriers, accounting for more than one-third of the world's carriers and up to 30 million chronic hepatitis B patients.[5] These data suggest that HBV has not only not disappeared but also continues to infect people. Currently, there are no drugs that effectively treat hepatitis B patients or HBV carriers, so timely and planned hepatitis B vaccination is the most effective way to prevent HBV infection.[6] Currently, available recombinant HBsAg subunit vaccines, which are safer than inactivated or live attenuated vaccines but carry the potential risk of virulence atavism and are less immunogenic, need to be supplemented with adjuvants to induce a good immune response. The utilization of aluminum as an adjuvant is prevalent in commercial antiviral-hepatitis B vaccines. Although aluminum adjuvant enhances the humoral immune response, it has difficulty in activating effector $CD4^+$ or $CD8^+$ T cells. Therefore, clearing intracellularly infected viruses and producing the synergistic protective effect of humoral and cellular immunity are challenging. Aluminum adjuvants are also prone to side effects, such as inflammatory reactions, granulomas, and subcutaneous nodules.[7−9] In addition, the stability of the current hepatitis B vaccines is inadequate. This means that during production, storage, transportation, and clinical vaccination, the vaccine must be kept at a cold storage or freezing temperature, referred

Received: November 1, 2023
Revised: January 23, 2024
Accepted: January 23, 2024

Scheme 1. Schematic Illustration of the Preparation of HZ and HSZ to Enhance Vaccine Stability and Induce Humoral and Cellular Immune Responses In Vivo and In Vitro; (A) 2-Methylimidazole (MeIM), HBsAg, and Zinc Acetate were Mixed Together to Produce HZ, Which was Then Modified with SF; The Synthesized HSZ Improved the Thermal Stability of HBsAg and Facilitated RT Storage; (B) After Intramuscular Injection of HSZ in Mice, an Antigenic Reservoir at the Injection Site Forms, Strong Antigen-Specific Humoral and Cellular Immune Responses are Induced, and Immune Memory is Enhanced

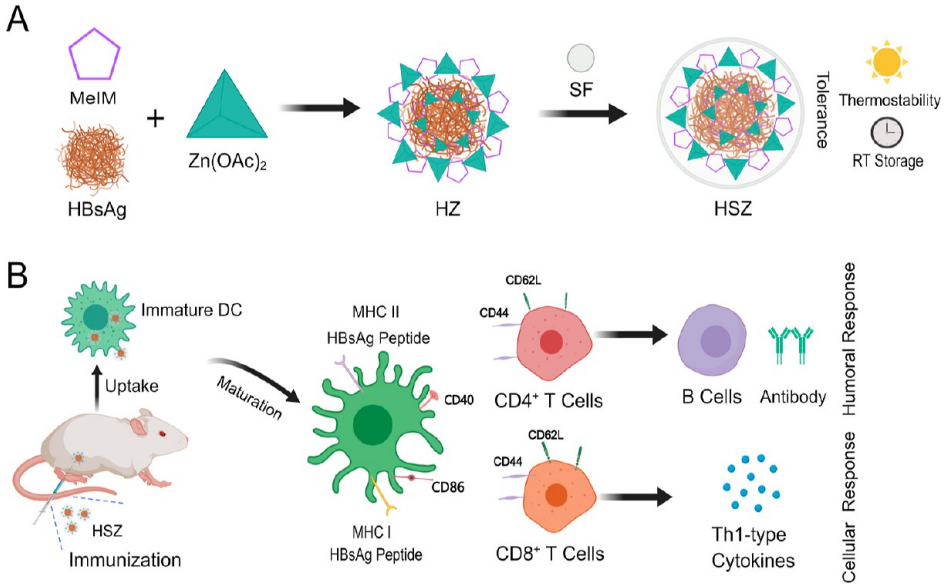

to as the vaccine cold chain. Notably, elevated temperatures lead to the degradation of HBsAg in the vaccine, destroying its intricate composition and impeding the successful elicitation of an enhanced immune protective response after vaccination.[10,11] Moreover, the vaccine cold chain accounts for approximately 80% of the total cost of vaccination programs, resulting in approximately 50% of vaccine products being discarded each year.[12,13] The vaccine cold chain increases not only the risk of vaccine failure but also the cost of vaccines. As a result, attempts have been made to increase the thermal stability of vaccines to extend their storage duration and reduce their dependence on the cold chain.

The safety, heat resistance, and stability of vaccines are critical factors that significantly impact their utilization. Since the outbreak of coronavirus disease 2019 (COVID-19), there has been a substantial surge in the global demand for vaccination. However, insufficient cold chain transport and storage facilities have significantly restricted the utilization of COVID-19 vaccines in certain countries and regions.[14] It is challenging to vaccinate individuals in remote locations with the currently available commercial hepatitis B vaccine due to the lengthy vaccination cycle, which also hinders efficient HBV prevention and management. In addition, to prevent perinatal transmission of HBV, the World Health Organization recommends that infants receive their first dose of hepatitis B vaccine within 24 h of birth, but this is also a challenge in some remote areas or countries that lack or have an inadequate vaccine cold chain. Although some regions or countries, such as rural China, rural Vietnam, the Solomon Islands and Lao People's Democratic Republic, have implemented strategies such as storing hepatitis B vaccines outside the cold chain to alleviate the burden on the cold chain, it remains essential to address the problem of the vaccine cold chain by fundamentally enhancing the thermal stability of vaccines.[15−18] Currently, the predominant approaches employed to enhance the thermal stability of vaccines involve the utilization of stabilizers, such as polyethylene glycol (PEG),[19] glutamate,[20] and alginate,[21] as well as thermal stabilization techniques, including genetic engineering,[22] surface charge engineering,[23] freeze-drying,[24] spray-drying,[25] and foam-drying.[26] In recent years, several innovative approaches have been developed for the manufacture of vaccines that can withstand high temperatures, including the use of gold nanoparticles,[27] bacterial spores,[28] poly(lactic-*co*-glycolic acid) particles,[29] and virus-like particles.[30] Unfortunately, these approaches still rely on the cold chain or have intricate preparation processes, which limit their application. In addition, using the most advanced delivery method for mRNA vaccines to date, nanostructured lipid carriers (NLCs) also improve the thermal stability of vaccines. Self-amplifying RNAs (saRNAs) can be coupled with NLCs to create a saRNA/NLC vaccine, which can be lyophilized and stored at room temperature (RT) for at least 6 months or stored at 4−8 °C for at least 10 months. However, several problems remain for their clinical use, such as poor immunological function, inability to be taken up by cells, difficulty in loading large molecular drugs, and susceptibility to particle size expansion and flocculation during long-term storage.[31,32]

Metal−organic frameworks (MOFs) are a class of porous materials with a crystalline structure formed by the self-assembly of metal ions and organic ligands through ligand bonding. MOFs are widely used in gas storage and separation, catalysis, sensing, and biomedicine due to their ease of preparation, tuneable and uniform pore sizes, large specific surface area, and good biocompatibility.[33−35] Due to these numerous advantages, MOFs are mainly used in biomedical applications for drug delivery (encapsulation, oral, and ocular delivery), in vivo photothermal and radiotherapy, diagnosis (glioma, prostate cancer, and early diagnosis of Alzheimer's disease), magnetic resonance imaging, and optical imaging and as vaccine carriers, antimicrobial agents, etc. Furthermore, MOFs can be modified after synthesis, such as with PEG, by

https://doi.org/10.1021/acsami.3c16358
ACS Appl. Mater. Interfaces XXXX, XXX, XXX−XXX

postsynthetic modifications based on metals or ligands, and by postsynthetic guest substitution in the MOFs, making MOFs one of the most promising materials for future biomedical applications.[36] In recent years, zeolitic imidazolate framework-8 (ZIF-8), which is composed of zinc ions and 2-methylimidazole, has garnered attention due to the excellent properties of MOFs and its sensitive response to pH. Consequently, ZIF-8 has been explored as a potential framework to protect various encapsulated model proteins, such as ovalbumin,[37] bovine serum albumin,[38] and tobacco mosaic virus.[39] Using ZIF-8 as a platform to disrupt the vaccine cold chain by implementing nano-MOFs has attracted considerable attention. Silk fibroin (SF) is a bioderived protein extracted from silkworm cocoons that has good biocompatibility, controlled biodegradability, and low immunogenicity, which allow it to enter the body with a minimal inflammatory response.[40,41] A recent study investigated the application of air-dried thin films containing SF for polio vaccine protection. After nearly 3 years of storage at RT, 70% of the antigenic potency of poliovirus D remained. Furthermore, after 1 year of storage at 45 °C, the potency of the IPV-2 and IPV-3 serotypes exceeded 50%.[42] Due to the aforementioned beneficial properties of SF coatings, they have the potential to facilitate the development of heat-resistant vaccines and offer ideas for vaccine storage at RT. However, few studies have investigated the use of SF-coated nano-MOFs to enhance the thermostability and immunogenicity of vaccines.

Herein, we developed two straightforward and flexible approaches to encapsulate HBsAg into ZIF-8 in aqueous solution, followed by modification with SF to produce HBsAg/SF@ZIF-8 (HSZ) (Scheme 1). Compared to aluminum adjuvants, HSZ exhibited enhanced thermostability at elevated temperatures and induced more robust immune responses in vivo and in vitro. Subsequent research showed that HSZ can act in a variety of ways, including increasing antigen loading, enhancing the positive zeta potential, improving the antigen-presenting cells (APCs) uptake efficiency, enabling pH-responsive release, facilitating antigen escape from lysosomes, promoting memory T-cell responses, and establishing an antigen reservoir at the injection site. Notably, HSZ exhibited a nearly equivalent capacity to the untreated group in terms of inducing cellular and humoral immune responses 14 days after storage at 25 °C. We expect that SF-coated nano-MOFs will provide insights on how to break the cold chain of vaccines so that vaccines can be stored at RT.

EXPERIMENTAL SECTION

Materials. 2-Methylimidazole (99%) and zinc acetate [$Zn(OAc)_2$, 99.99%] were purchased from Sigma-Aldrich (USA). HBsAg and enzyme-linked immunosorbent assay (ELISA) kits for HBsAg, IgG, IgG1, and IgG2a were purchased from Ruixin Biotech (Quanzhou, China). SF was purchased from Aladdin (Shanghai, China). Recombinant mouse IL-4 and granulocyte-macrophage colony-stimulating factor (GM-CSF) were purchased from R&D Systems (USA). BCA protein assay kits were purchased from Thermo Fisher Scientific (San Diego, USA). The CellTiter 96 AQueous One Solution Cell Proliferation Assay (MTS) kit was purchased from Promega (USA). A Quick FITC antibody (protein) labeling kit was purchased from MeilunBio (Dalian, China). A Cy5.5 antibody conjugation kit and Rehydragel@LV alum adjuvant were purchased from Bioss (Beijing, China). ELISA kits for IL-2, IL-4, IL-5, IL-6, IL-10, IL-12, IL-12p70, TNF-α, and IFN-γ were purchased from Mlbio (Shanghai, China). All fluorochrome-conjugated antimouse antibodies for flow cytometry were purchased from BioLegend (USA). All other reagents used were of analytical grade.

Synthesis of FITC/Cy5.5-HBsAg. HBsAg was labeled using Quick FITC Antibody (Protein) labeling and Cy5.5 antibody conjugation kits according to the instructions.

Preparation of ZIF-8, HZ, and HSZ Composites. A modified procedure was used to prepare ZIF-8 and HBsAg@ZIF-8 (HZ) in deionized water by two methods.[30,35] Briefly, to prepare HZ by the one-pot shake method (three-step shake method), abbreviated as HZ-1, 450 μL of 2-methylimidazole (80 mM) and 100 μL of HBsAg (1 mg/mL) were quickly mixed, then added to 50 μL of zinc acetate (20 mM), and the mixture was shaken (500 rpm/min) on an oscillator for 10 min at 4 °C. Equal amounts of 2-methylimidazole and zinc acetate were added to the mixture, and shaking was continued for 20 min at 4 °C. After ultrasonic dispersion for 5 min, 20 μL of 2-methylimidazole (2 M) and 6 μL of zinc acetate (200 mM) were added, and the mixture was shaken for 1 h at 4 °C. Next, the samples were centrifuged (10,000 rpm, 5 min), washed three times with deionized water, and vacuum-dried at RT. The collected supernatant was analyzed, and the amount of HBsAg encapsulated in ZIF-8 was calculated using a BCA protein assay kit.

To prepare HZ by the one-step shake method, abbreviated as HZ-2, 100 μL of 2-methylimidazole (320 mM) and 200 μL of HBsAg (0.5 mg/mL) were rapidly mixed and then added to 100 μL of zinc acetate (80 mM); the mixture was shaken (500 rpm/min) on an oscillator for 40 min at 4 °C. Next, the samples were centrifuged (10,000 rpm, 5 min), washed three times with deionized water, and dried under vacuum at RT.

Additional modifications to the preparation method of Wang et al. were made.[41] To prepare HBsAg/SF@ZIF-8−1 (HSZ-1) or HBsAg/SF@ZIF-8−2 (HSZ-2), 1 mg of HZ-1 or HZ-2 was resuspended in 200 μL of deionized water. Then, 10 μL of 0.1% (w/v) SF was added to the suspension. The mixture was shaken (600 rpm/min) on an oscillator for 2 min at RT. After ultrasonic dispersion for 2 min, the samples were shaken for an additional 2 min at RT. Next, the samples were centrifuged (12,000 rpm, 5 min), washed three times with deionized water, and dried under vacuum at RT.

Characterization. The nanoparticle morphology was observed by scanning electron microscopy (SEM, TESCAN MAIA3, Czech Republic). The hydrodynamic diameter and zeta potential of the nanoparticles were measured using a Zetasizer Nano instrument (Malvern ZS90, UK). Fourier transform infrared (FT-IR) spectra analyses were performed using a Nicolet 6700 spectrometer (Thermo Fisher Scientific, USA). X-ray measurements were performed using an X-ray diffractometer (XRD, SmartLab, Japan). The HZ and HSZ were soaked in 10% SDS washing solution for 10 min, then centrifuged, and washed three times with deionized water. After the addition of EDTA exfoliation buffer,[39] the amount of HBsAg encapsulated in the nanoparticles was calculated using a BCA protein assay kit.

Cytotoxicity. The cytotoxicities of ZIF-8, HZ, and HSZ were evaluated by an MTS assay. Briefly, RAW264.7 macrophages and DC2.4 cells (2×10^4 cells per well) in 100 μL of medium were seeded onto 96-well plates and incubated at 37 °C for 24 h before various concentrations of ZIF-8, HZ, or HSZ (ranging from 0 to 100 mg/mL) were added for an additional 24 h of incubation. Next, 20 μL of the MTS reagent was added to each well for 1.5 h of incubation. Finally, the absorbance at 490 nm was measured by using a microplate reader (Tecan, Austria).

Hemolysis Assay. Mouse blood was collected, and the red blood cells were separated by centrifugation (1000 rpm, 10 min), washed three times with PBS, and made into a 2% erythrocyte suspension. Then, 500 μL of different concentrations of HZ and HSZ (25, 50, 100, 200, 300, 400, and 500 μg/mL) was added to an equivalent volume of 2% erythrocyte suspension, with PBS as the negative control and 0.2% Triton X-100 as the positive control. The various combined solutions were incubated at 37 °C for 1 h. After centrifugation, the samples were photographed, and the supernatant was collected. The absorbance of each supernatant sample was measured using an UV−vis absorption spectrophotometer to identify red blood cell hemolysis at different HZ and HSZ concentrations.

https://doi.org/10.1021/acsami.3c16358
ACS Appl. Mater. Interfaces XXXX, XXX, XXX−XXX

HBsAg Release In Vitro. The in vitro release of HBsAg from HZ and HSZ was studied in PBS solutions (pH = 7.4, 6.5, and 5.0) at 37 °C with shaking (400 rpm). The supernatants of HZ-1, HSZ-1, HZ-2, and HSZ-2 were collected by centrifugation (10,000 rpm, 5 min) at the desired time points (0.5, 1, 2, 4, 6, 8, 12, and 24 h), and the HBsAg released into the supernatant was quantified by a BCA assay kit.

Thermostability Determination. To investigate the thermal stability of HZ and HSZ, they were suspended in deionized water and incubated at 37, 45, and 60 °C for 1, 6, and 12 h and placed on ice as a control (named as 0 °C). The samples were treated with an EDTA exfoliation buffer, and the proteins released into the supernatant were collected by centrifugation (10,000 rpm, 10 min). The activity of HBsAg was determined by ELISA kits. In addition, to study the long-term stability of the nanoparticles, these samples were stored at 25 °C and 45−65% relative humidity in a drug comprehensive stability test chamber (Zuocheng Instruments, China) for 7, 14, 21, and 28 days. HBsAg activity was determined by ELISA kits after treatment with an EDTA exfoliation buffer.

Solution Stability Determination. HZ and HSZ were placed in different solutions of DMEM, normal saline, and simulated body fluid (SBF). Samples were taken at different intervals (6, 12, and 24 h), and the HBsAg released into the supernatant was quantified by a BCA assay kit.

Isolation and Cultivation of BMDCs. Bone marrow-derived DCs (BMDCs) were obtained from SPF male BALB/c mice. The femurs and tibias of the mice were removed and immersed in 75% ethanol for 5 min. To obtain the desired cells, the bone marrow was flushed with RPMI 1640 medium using a 1 mL sterile syringe alternately on both sides until the bone became translucent, and the cells were filtered through a 100-mesh sieve. The cell suspension was centrifuged at 1500 rpm for 5 min, and the cells were then resuspended in 3 mL of an erythrocyte lysis solution for 5 min. After terminating lysis with RPMI 1640 medium and centrifugation, the cells were grown in RPMI 1640 medium with 10% FBS, 1% penicillin−streptomycin, 20 ng/mL GM-CSF, and 20 ng/mL IL-4 at 37 °C under 5% CO_2; this day was designated day 0. After 2 days, all media were replaced with fresh media. On days 4 and 6, half of the medium was replaced with fresh medium. On day 7, the suspended cells, the extracted BMDCs, were collected.

Cellular Uptake. To analyze the cellular uptake, FITC-labeled HBsAg was prepared as previously described. Briefly, RAW264.7 macrophages, DC2.4 cells, and BMDCs were seeded in 12-well plates at a density of 1×10^5 cells per well and treated with HBsAg, Alum + HBsAg (a 1:2 mixture of HBsAg and aluminum adjuvant), HZ-1, HSZ-1, HZ-2, or HSZ-2 at a final FITC-HBsAg concentration of 5 μg/mL. After 6 h of incubation, the cells were washed three times with staining buffer (PBS containing 2% bovine serum albumin and 1% penicillin−streptomycin) and analyzed using a flow cytometer (BD, USA). The DC2.4 cells were stained with Hoechst 33342 (2.5 μg/mL) in the dark at RT for 15 min. Subsequently, the cells were washed three times with PBS and observed by confocal laser scanning microscopy (CLSM, Olympus, Japan).

Lysosomal Escape. DC2.4 cells were seeded on 12-well plates at a density of 1×10^5 cells per well and then cocultured with HBsAg, Alum + HBsAg, HZ-1, HSZ-1, HZ-2, or HSZ-2 (at a final FITC-HBsAg concentration of 5 μg/mL) for 12 h. Cells were then stained with LysoTracker Red and Hoechst 33342, washed three times with PBS, and observed by CLSM.

Activation of BMDCs. BMDCs were seeded on 12-well plates at a density of 1×10^6 cells per well and then cocultured with HBsAg, Alum + HBsAg, HZ-1, HSZ-1, HZ-2, or HSZ-2 (at a final HBsAg concentration of 5 μg/mL) for 24 h. Cells incubated with PBS were used as a negative control. The cells were washed three times with staining buffer and then stained with APC-anti-CD11c, FITC-anti-CD86, and PE-anti-CD40 antibodies for 45 min at 4 °C in the dark. The cells were then washed twice with staining buffer and analyzed with a flow cytometer.

In Vitro Cytokine Assays. RAW264.7 macrophages and immature BMDCs were seeded in 12-well plates at a density of 1×10^5 cells per well and then cocultured with HBsAg, Alum + HBsAg, HZ-1, HSZ-1, HZ-2, or HSZ-2 (at a final HBsAg concentration of 5 μg/mL) for 24 h. The supernatant was collected, and the levels of IL-6 and TNF-α from the RAW264.7 macrophages and IL-12p70 from the BMDCs were assessed using ELISA kits.

Animal Immunization. SPF BALB/c mice (6−8 weeks old) were purchased from Liaoning Changsheng Biotechnology Co., Ltd. All animal experiments were performed in accordance with the Guide for the Care and Use of Laboratory Animals and obtained permission from Experimental Animal Ethics Committee in Jilin Agricultural University (approval number: 2023 06 06 001).

SPF female BALB/c mice were randomly assigned to 13 groups (n = 5): PBS (control), HBsAg, Alum + HBsAg, HZ-1, HSZ-1, HZ-2, HSZ-2, HBsAg (stored at 25 °C for 14 days, named heat treatment), Alum + HBsAg (heat), HZ-1 (heat), HSZ-1 (heat), HZ-2 (heat), and HSZ-2 (heat). On days 0, 14, and 28, mice were intramuscularly injected with 100 μL of various agents containing 10 μg of HBsAg. Blood was collected from the tail vein on days 14, 21, 28, and 35 after the initial vaccination.

Antibody Detection. An indirect ELISA approach was used to assess HBsAg-specific antibodies IgG, IgG1, and IgG2a in serum.

Analysis of Splenocyte Proliferation. Mice splenocytes were harvested 35 days after immunization and plated in a 96-well plate at a density of 1×10^5 cells per well. Then, HBsAg was added to a final concentration of 5 μg/mL. Culture medium was used as a blank control, while the group without the HBsAg addition was used as a negative control. Each sample consisted of three replicates. The cells were cultured for 48 h at 37 °C in 5% CO_2. Then, 20 μL of the MTS reagent was added to each well, and the incubation was continued for 1.5 h. The absorbance at 490 nm was then measured by using a microplate reader.

Splenocyte Activation and the Memory T-Cell Response. The collected splenocytes were plated in 24-well plates at a density of 1×10^6 cells per well and treated with HBsAg (5 μg/mL) for 48 h. The cells were then centrifuged at 4 °C for 10 min at 1500 rpm, and the levels of the cytokines TNF-α, IFN-γ, IL-2, IL-4, IL-5, IL-6, IL-10, and IL-12 in the supernatants were measured using ELISA kits. Cells were washed three times with staining buffer and then stained with PE-anti-CD3, APC-anti-CD4, APC-anti-CD8a, FITC-anti-CD44, and PerCP/Cy5.5-anti-CD62L antibodies for 45 min at 4 °C in the dark. The cells were then washed twice with staining buffer and analyzed using a flow cytometer.

Fluorescence Imaging of the Injection Site. SPF BALB/c mice were divided into six groups (n = 3): HBsAg, Alum + HBsAg, HZ-1, HSZ-1, HZ-2, and HSZ-2. The mice were intramuscularly injected with 100 μL of the appropriate agent, each containing 10 μg of Cy5.5-HBsAg. Mice were anaesthetized and photographed using a small animal fluorescence imaging system (Berthold, Germany) at predetermined time points (0, 2, 6, 12, 24, 48, 72, 96, and 120 h).

Biodistribution of HSZ. The HSZ-1 and HSZ-2 were injected into mice by intramuscular or tail vein injection, while uninjected mice were used as controls. After injection, mice were sacrificed either 5 or 2 days later, and zinc levels in major organs (heart, liver, spleen, lung, kidney, or muscle) were measured by inductively coupled plasma-mass spectrometry (ICP-MS, Aglient, USA).

Viscera Indices, Histopathological Assay, and Biochemical Indices. Mice were sacrificed 35 days after vaccination to collect vital organs (including heart, liver, spleen, lung, and kidney), which were then weighed, and the viscera indices were calculated. The organs were then embedded in paraffin and subjected to the histopathological examination using hematoxylin-eosin staining. The mice serum was separated to determine various biochemical indices, including aspartate aminotransferase, alanine transaminase, alkaline phosphatase, total bilirubin, globulin, lactate dehydrogenase, creatine kinase, blood urea nitrogen, and creatinine.

Statistical Analysis. All statistical analyses were performed by using GraphPad Prism 9 or SPSS 16.0 software, and all data are expressed as the mean ± SD (n = 3). Differences between two groups were determined by using an independent-sample t-test or one-way ANOVA for multiple group comparisons. Significant differences

https://doi.org/10.1021/acsami.3c16358
ACS Appl. Mater. Interfaces XXXX, XXX, XXX−XXX

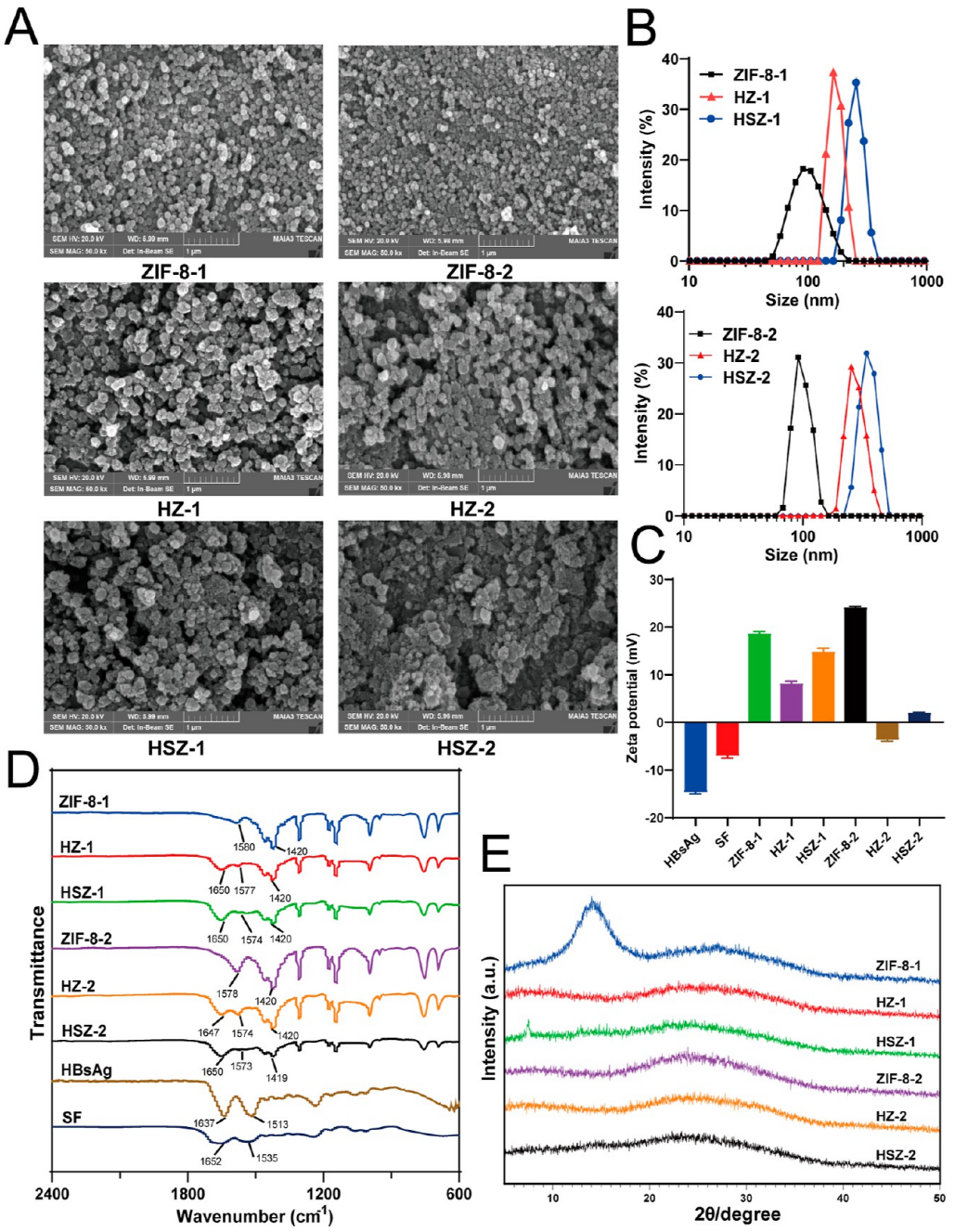

Figure 1. Characterization of ZIF-8, HZ, and HSZ. (A) SEM images of ZIF-8, HZ, and HSZ. (B,C) Hydrated particle sizes and zeta potentials of ZIF-8, HZ, and HSZ were determined by DLS. (D) FT-IR spectra of ZIF-8, HZ, and HSZ. (E) XRD patterns of ZIF-8, HZ, and HSZ.

between the groups were expressed as follows: $*p < 0.05$, $**p < 0.01$, $***p < 0.001$, $****p < 0.0001$; and ns: no significant difference.

RESULTS AND DISCUSSION

Synthesis and Characterization. ZIF-8, HZ, and HSZ were prepared in aqueous solution by the one-pot shake method and the one-step shake method. According to the SEM measurements, the obtained ZIF-8 nanoparticles had a uniform shape and good dispersion, with a particle size of approximately 100 nm. The shape of the nanoparticles loaded with HBsAg and modified with SF was comparable to that of ZIF-8, but the loaded particles had a rougher surface and were larger, measuring between 200 and 300 nm (Figure 1A). DLS analysis showed that the particle sizes of ZIF-8−1, HZ-1, HSZ-1, ZIF-8−2, HZ-2, and HSZ-2 were 93, 158, 223, 95, 244, and 329 nm, respectively (Figure 1B), and the zeta potentials were 18.7 ± 0.36 mV, 8.25 ± 0.39 mV, 14.85 ± 0.69 mV, 24.7 ± 0.15 mV, −3.66 ± 0.29 mV, and 2.02 ± 0.09 mV, respectively (Figure 1C). After loading HBsAg, the zeta potential decreased significantly, indicating that negatively charged HBsAg was successfully encapsulated in ZIF-8. Interestingly, although the SF itself had a negative charge, the modification of HZ with the SF coating increased the positive zeta potential. The SF molecule contains a hydrophobic and a hydrophilic peptide chain with specific amino acid sequences, forming a variety of secondary conformations, and the diverse structures can be converted into each other. During the HSZ preparation process, the application of shaking and sonication may induce

https://doi.org/10.1021/acsami.3c16358
ACS Appl. Mater. Interfaces XXXX, XXX, XXX−XXX

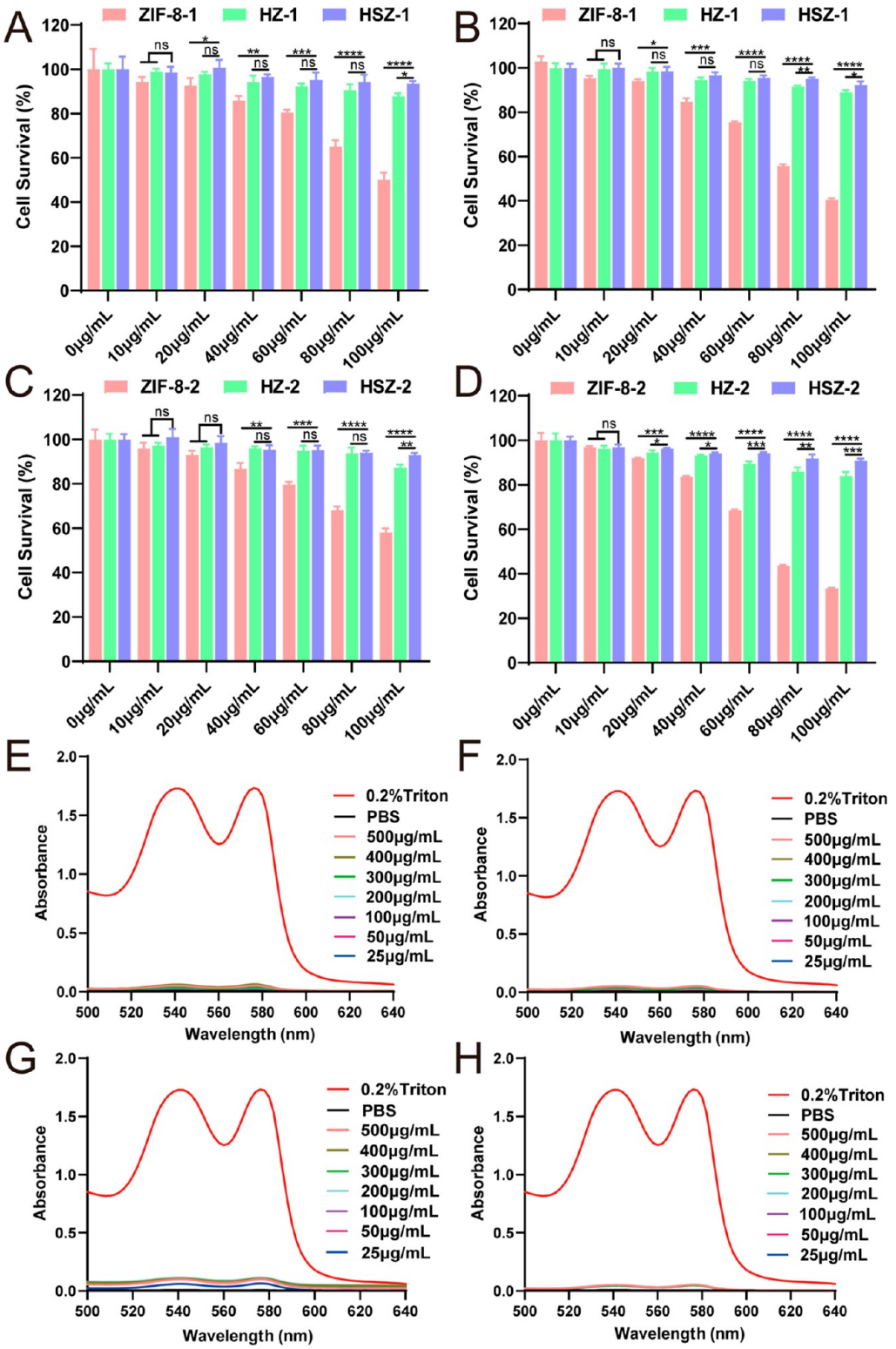

Figure 2. Biocompatibility of ZIF-8, HZ, and HSZ. (A,B) MTS assay results of toxicity to RAW264.7 macrophages and DC2.4 cells after 24 h of treatment with ZIF-8−1, HZ-1, and HSZ-1. (C,D) MTS assay results of toxicity to RAW264.7 macrophages and DC2.4 cells after 24 h of treatment with ZIF-8−2, HZ-2, and HSZ-2. Determination of the absorption peaks of hemoglobin in the supernatants of RBCs treated with (E) HZ-1, (F) HSZ-1, (G) HZ-2, and (H) HSZ-2 by UV−vis spectroscopy. The data are presented as the mean ± SD (n = 3). *p < 0.05, **p < 0.01, ***p < 0.001, ****p < 0.0001; and ns: no significant difference.

transitions between the different SF structures, which in turn could alter the zeta potential. The FT-IR spectroscopy data showed that the amides I (1680−1630) and II (1650−1515) were observed in HBsAg, SF, HZ, and HSZ, respectively, indicating that HBsAg was successfully encapsulated in HZ and that SF coating modification of HZ was successful (Figures 1D and S1). The XRD profiles showed that the diffraction peaks of HZ-1 and HSZ-1 were almost identical to that of ZIF-8−1 in

https://doi.org/10.1021/acsami.3c16358
ACS Appl. Mater. Interfaces XXXX, XXX, XXX−XXX

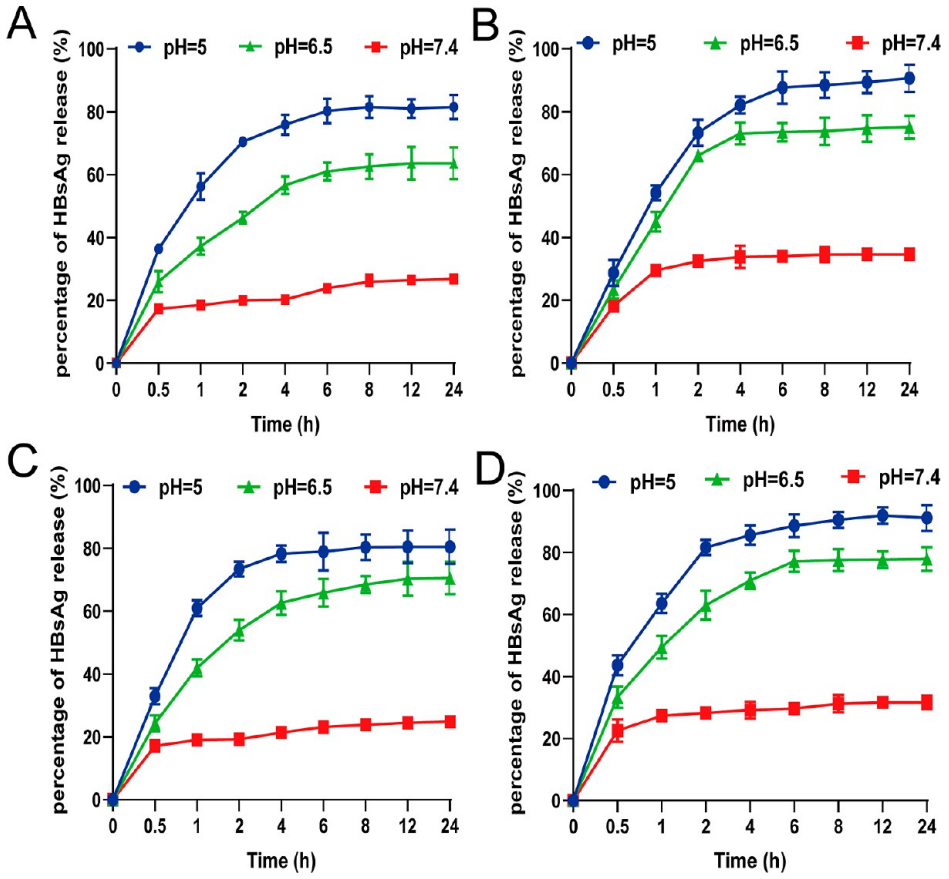

Figure 3. Release profiles of HBsAg at different pH values. In vitro HBsAg release from (A) HZ-1, (B) HSZ-1, (C) HZ-2, and (D) HSZ-2 in PBS at pH 7.4, 6.5, and 5.0. The data are presented as the mean ± SD (n = 3).

2θ values, with only minor variations in intensity. Similarly, the diffraction peaks of ZIF-8−2, HZ-2, and HSZ-2 showed almost identical patterns. This indicates that HBsAg encapsulation and SF coating modification did not affect the structure of ZIF-8 (Figure 1E). The BCA protein assay kit results showed 70.6% encapsulation efficiency by the one-pot shake method and 90.7% encapsulation efficiency by the one-step shake method (Figure S2). After soaking in 10% SDS washing solution, more than 90% of the HBsAg remained in the HZ and HSZ. This indicates that most of the HBsAg is encapsulated within the nanoparticles rather than attached to the outer surface of the particles, whether the one-pot shake method or the one-step shake method is used (Figure S3).

Assessment of Cytotoxicity and Hemolytic Activities In Vitro. When nanovaccines are developed, biocompatibility is one of the most critical considerations. We first investigated the toxicity of ZIF-8−1, HZ-1, HSZ-1, ZIF-8−2, HZ-2, and HSZ-2 to RAW264.7 macrophages and DC2.4 cells using the MTS assay. As shown in Figure 2A−D, when the concentration of HZ-1 and HSZ-1 groups reached 100 μg/mL, the cell survival rates were higher than 88 and 92%, respectively. In contrast, the cell survival rate in the ZIF-8−1 group was only 40%. When the concentration of HZ-2 and HSZ-2 groups reached 100 μg/mL, the cell survival rates were higher than 84 and 90%, respectively, whereas the cell survival rate in the ZIF-8−2 group was only 33%. This indicated that the toxicities of HZ-1 and HSZ-1 groups were slightly lower than those of the HZ-2 and HSZ-2 groups. In addition, the SF coating further reduced cytotoxicity and improved biocompatibility.

In addition, the hemolytic activity of nanovaccines is a significant factor in biocompatibility assessments. The results depicted in Figure 2E−H demonstrate that even at concentrations as high as 500 μg/mL, HZ-1, HSZ-1, HZ-2, and HSZ-2 groups did not cause hemolysis, which was consistent with the hemolysis test photographs (Figure S4), indicating that these nanoparticles do not induce any hemolytic effects in animals. The aforementioned data indicate that due to their robust biocompatibility, HZ and HSZ have the potential for application in the development of novel nanovaccines.

Release of HBsAg In Vitro in a pH-Responsive Manner. Antigen release from cells plays a crucial role in triggering the immunological response. To evaluate antigen release from HZ and HSZ, these materials were dispersed with PBS at different pH values (pH = 7.4, 6.5, and 5.0). As shown in Figure 3A−D, at pH 7.2, less than 25% of HBsAg was released from HZ-1 and HZ-2 groups within 24 h, while HBsAg release from HSZ-1 and HSZ-2 groups was less than 35% within 24 h. However, as the pH decreased, more HBsAg was released. At pH 6.5, approximately 70% or 80% of the HBsAg was released from the HZ-1 and HZ-2 or HSZ-1 and HSZ-2 particles within 24 h. At pH 5.0, more than 80% or 90% of the HBsAg was released from the HZ-1 and HZ-2 groups or HSZ-1 and HSZ-2 groups particles within 24 h. Compared to HZ, the increased release of HSZ at pH 5.0 may be due to the higher hydrophilicity of SF in PBS. ZIF-8 consists of the organic ligand 2-methylimidazole and metal Zn^{2+}. The ligand and metal ion dissociate in acidic environments, leading to the release of antigens. These results suggest that HZ and HSZ can

https://doi.org/10.1021/acsami.3c16358
ACS Appl. Mater. Interfaces XXXX, XXX, XXX−XXX

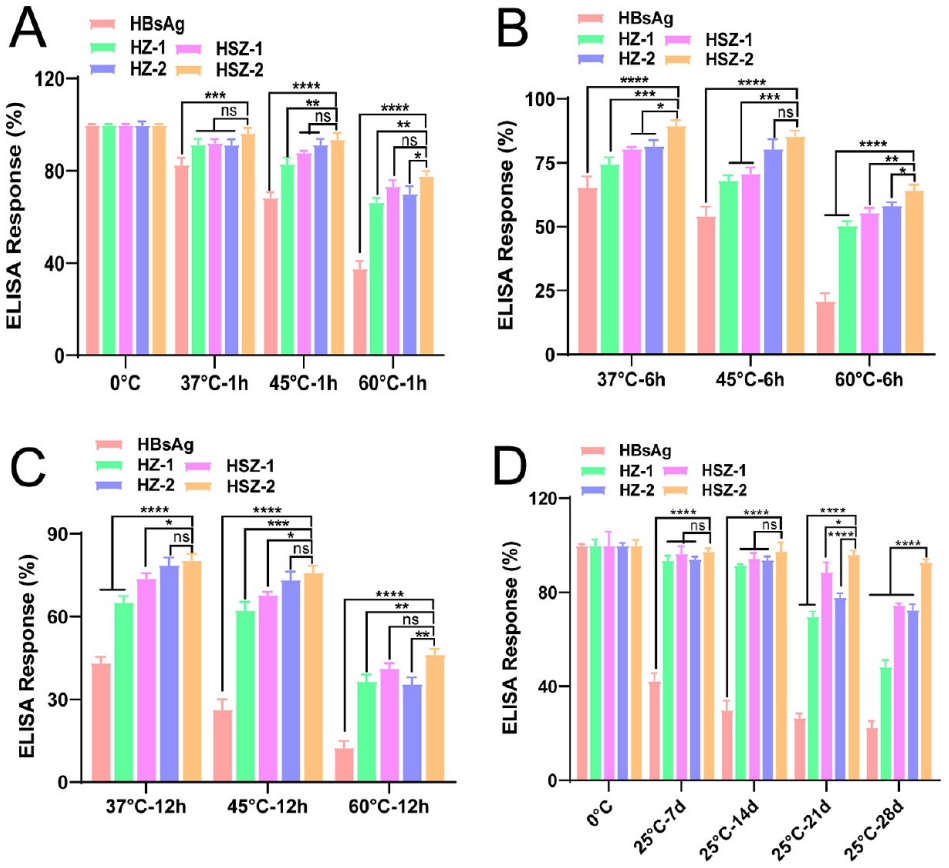

Figure 4. Thermostability of HBsAg, HZ, and HSZ. (A−C) Thermostability of HBsAg, HZ-1, HZ-2, HSZ-1, and HSZ-2 after treatment at 37, 45, and 60 °C for 1, 6, and 12 h determined by ELISA kits. (D) Evaluation of the effect of RT storage on the stability of HBsAg, HZ-1, HZ-2, HSZ-1, and HSZ-2 by ELISA kits. The data are presented as the mean ± SD (n = 3). *p < 0.05, **p < 0.01, ***p < 0.001, ****p < 0.0001; and ns: no significant difference.

be triggered to release antigens in a pH-responsive manner, which may enhance the ability of APCs to capture and present antigens, thereby promoting the subsequent immune response.

HZ and HSZ Improve the Thermostability of HBsAg. It has been reported that the SF coating increases the thermal stability of proteins. Therefore, we measured the activity of HBsAg in HZ and HSZ after treatment at different temperatures for different lengths of time using ELISA kits. As shown in Figure 4A−C, HBsAg activity decreased with increasing treatment temperature and time. After 1 h of treatment at 60 °C, HBsAg activity in the HZ-1 and HZ-2 groups remained at approximately 65%, whereas the activity in the HSZ-1 and HSZ-2 groups exceeded 73% but was only 37.8% in the HBsAg group. According to these findings, encapsulating HBsAg in ZIF-8 made the antigen more thermally stable, and the addition of an SF coating had the potential to make this effect even more pronounced. Next, to study the RT storage stability, the samples were stored at 25 °C for 7, 14, 21, and 28 days. As shown in Figure 4D, the HBsAg activity in the HZ-1, HSZ-1, HZ-2, and HSZ-2 groups was over 90% after 7 days of treatment, whereas the HBsAg activity in the HBsAg group was only 40%. These data show that the activity of HBsAg in the HZ-2 and HSZ-2 groups was higher than that in the HZ-1 and HSZ-1 groups, indicating that the nanoparticles prepared by the one-step shake method were superior to those prepared by the one-pot shake method. As a result, the SF-coated ZIF-8 could enhance the thermal stability of the internally encapsulated HBsAg, and the HBsAg activity could be maintained at high temperatures, providing a novel solution to overcome the problem of the vaccine cold chain.

Stability of HZ and HSZ in Different Solutions. Solution stability is an indicator that examines the stability of nanoparticles in different solutions. It is used to determine whether the encapsulated antigen will be released from the nanoparticles. The release of HBsAg from the HZ-1, HSZ-1, HZ-2, and HSZ-2 groups in DMEM, NaCl, and SBF after 6 h was found to be below 15, 20, and 35%, respectively (Figure S5). Furthermore, HBsAg release showed a gradual increase with time.

HZ and HSZ Enhance HBsAg Uptake by APCs. The uptake of loaded antigens by APCs (especially DCs and macrophages) as well as their processing and presentation is essential for immune activation, inducing the initial actions of the immune response. After encapsulation by ZIF-8, the majority of negatively charged antigens can become positively charged, and the binding of these antigens to negatively charged cell membranes can significantly enhance their uptake efficiency.[43] As displayed in Figure 5A−C, the percentages of HBsAg-positive cells in the HZ-1, HSZ-1, HZ-2, and HSZ-2 groups were significantly higher than those in the HBsAg and Alum + HBsAg groups. CLSM images also showed that Alum + HBsAg, HZ-1, HSZ-1, HZ-2, and HSZ-2 groups were significantly more taken up by DC2.4 cells than the HBsAg group (Figure 5D). This indicates that the negative charge and hydrophilicity of HBsAg hinder its ability to efficiently cross the cell membrane for internalization.[44] In contrast, APCs were

https://doi.org/10.1021/acsami.3c16358
ACS Appl. Mater. Interfaces XXXX, XXX, XXX−XXX

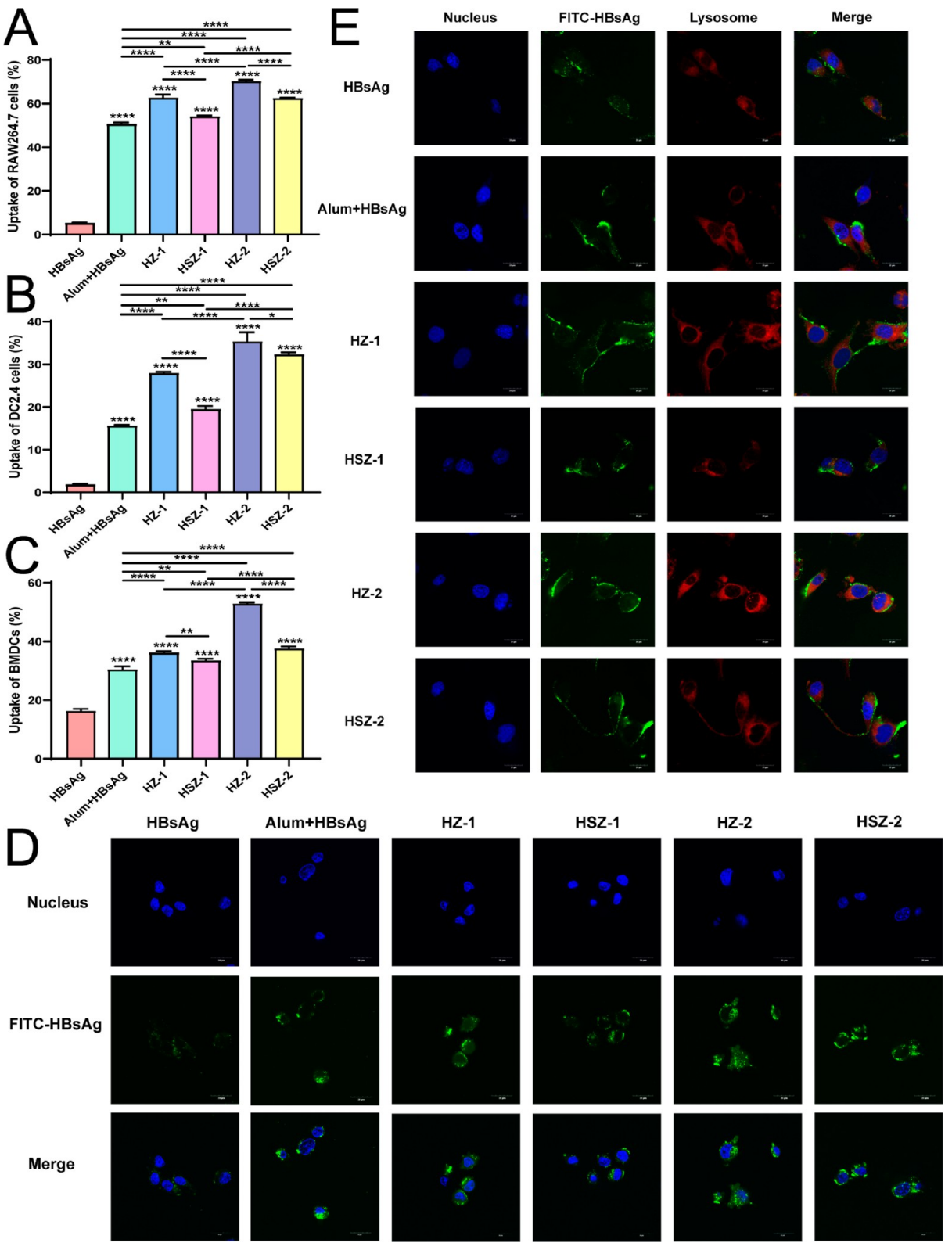

Figure 5. HZ and HSZ enhance HBsAg uptake and lysosomal escape. (A) RAW264.7 macrophages, (B) DC2.4 cells, and (C) BMDCs were cocultured with HBsAg, Alum + HBsAg, HZ-1, HSZ-1, HZ-2, and HSZ-2 (containing FITC-labeled HBsAg) for 6 h, and then cellular uptake was measured by flow cytometry. (D) Representative CLSM images of HBsAg, Alum + HBsAg, HZ-1, HSZ-1, HZ-2, and HSZ-2 taken up by DC2.4 cells. (E) Representative CLSM images of DC2.4 cells after 12 h of incubation with HBsAg, Alum + HBsAg, HZ-1, HSZ-1, HZ-2, and HSZ-2 to show lysosomal escape of the antigen. HBsAg was labeled with FITC (green). Nuclei and lysosomes were stained with Hoechst 33342 (blue) and LysoTracker (red), respectively. The data are presented as the mean ± SD (n = 3). *p < 0.05, **p < 0.01, ***p < 0.001, ****p < 0.0001; and ns: no significant difference.

https://doi.org/10.1021/acsami.3c16358
ACS Appl. Mater. Interfaces XXXX, XXX, XXX−XXX

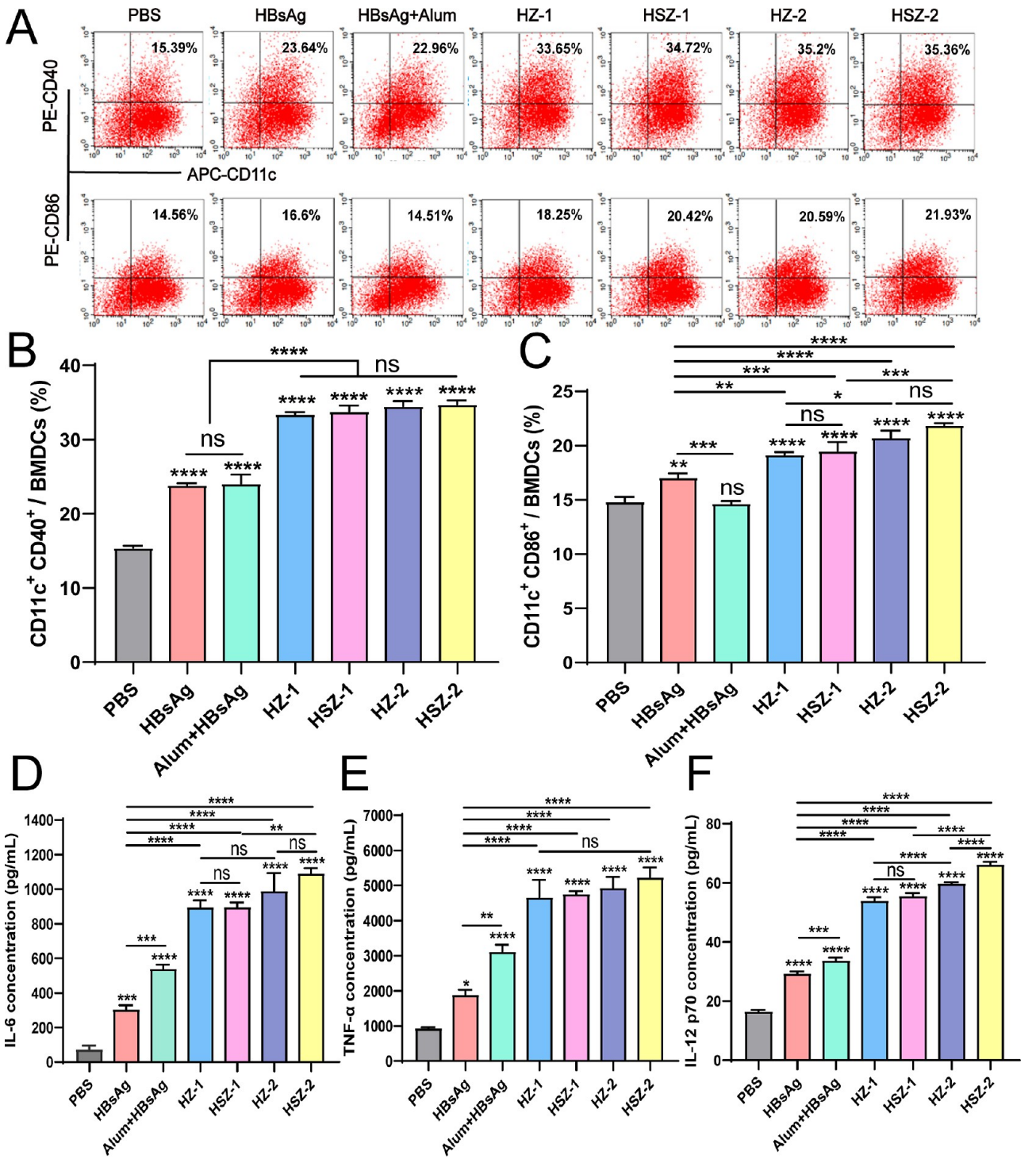

Figure 6. HZ and HSZ promote the activation of APCs. (A–C) Analysis of CD40 and CD86 expression on BMDCs by flow cytometry. (D–F) Secretion of the cytokines IL-6, TNF-α, and IL-12p70 by RAW264.7 macrophages and BMDCs was detected by ELISA kits. The data are presented as the mean ± SD (n = 3). *p < 0.05, **p < 0.01, ***p < 0.001, ****p < 0.0001; and ns: no significant difference.

shown to have a higher uptake of positively charged nanoparticles. The enhanced uptake of the nanovaccine by APCs may facilitate and improve antigen delivery and induce efficient humoral and cellular immunity.

HZ and HSZ Assisted in HBsAg Escape from Lysosomes. Exogenous antigens enter the cell and are processed via endosomal or lysosomal pathways to be delivered to major histocompatibility complex II (MHC II), where they are recognized by antigen-specific $CD4^+$ T cells to induce a B-cell immune response. Due to the proton sponge effect, ZIF-8 dissociates in the acidic lysosomal environment and rapidly releases the antigen, after which large quantities of ions and water enter the lysosome to trigger lysosomal rupture, allowing the antigen to enter the cytoplasm. However, the antigen that enters the cytoplasm can be identified as an endogenous substance, and after being processed by the proteasome pathway and presented to major histocompatibility complex I (MHC I), it can activate $CD8^+$ T cells and produce

https://doi.org/10.1021/acsami.3c16358
ACS Appl. Mater. Interfaces XXXX, XXX, XXX−XXX

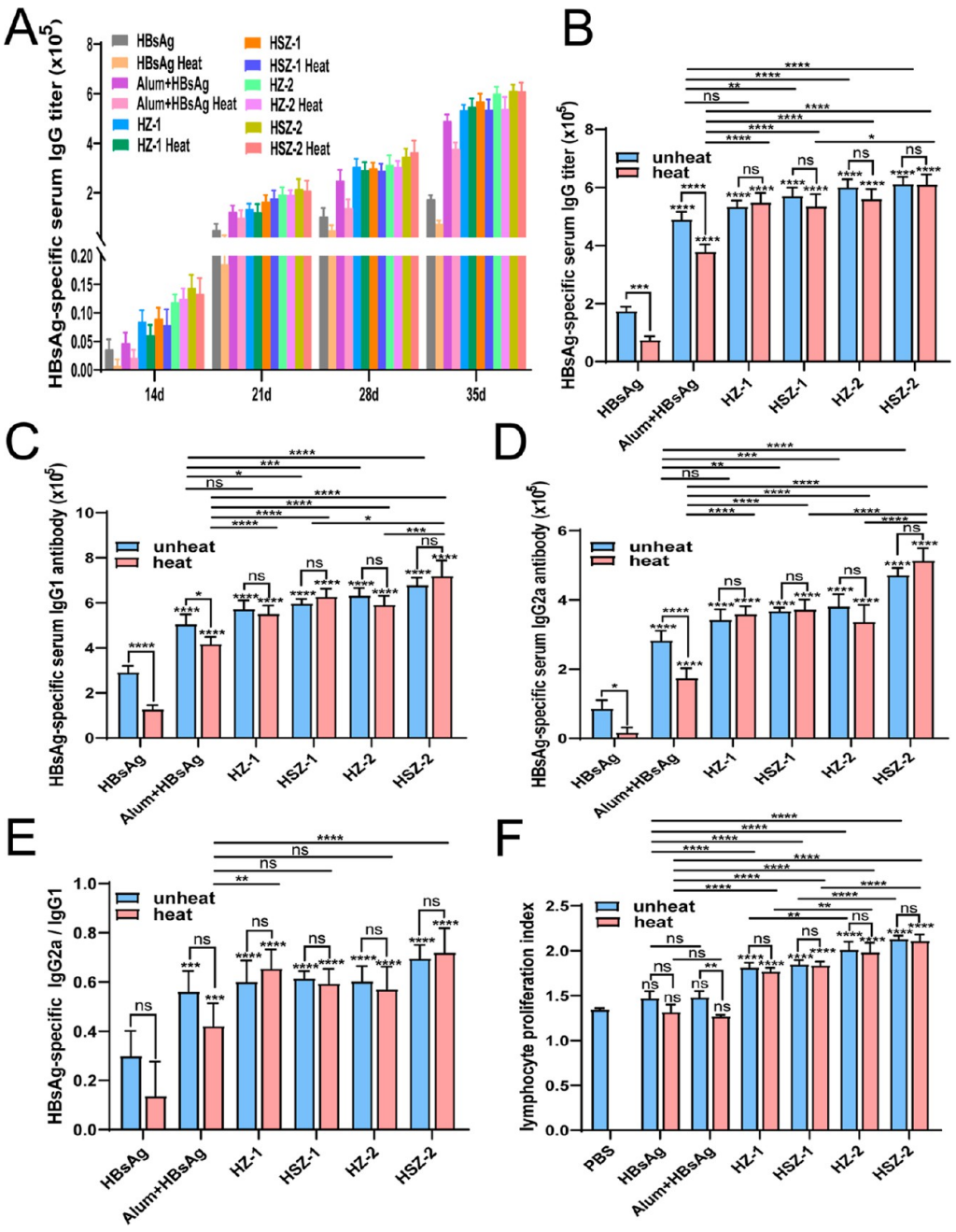

Figure 7. In vivo immune response before and after storage for 14 days at 25 °C. (A) HBsAg-specific IgG antibody titers were measured by ELISA kits at 14, 21, and 35 days after primary immunization. HBsAg-specific antibody (B) IgG, (C) IgG1, (D) IgG2a titers, and (E) IgG2a/IgG1 ratio on Day 35. (F) Splenocyte proliferation after restimulation with HBsAg in vitro. The data are presented as the mean ± SD (n = 5). *p < 0.05, **p < 0.01, ***p < 0.001, ****p < 0.0001; and ns: no significant difference.

specific cytotoxic T-lymphocytes (CTLs), thereby enhancing the cellular immune response and achieving antigen cross-presentation.[45] When the green fluorescence of HBsAg and the red fluorescence of the lysosome overlap to produce a yellow color, this means that HBsAg is still within the lysosome. Compared to the HBsAg group, the lysosomal antigen escape in the HZ-1, HSZ-1, HZ-2, and HSZ-2 groups was significantly higher (Figure 5E). This suggests that encapsulating HBsAg with ZIF-8 and SF enhances lysosomal escape. Therefore, SF-coated ZIF-8 promotes antigen cross-presentation and is expected to induce a synergistic B-cell and T-cell immune response.

HZ and HSZ Promote APCs Activation. Following antigen uptake, DCs progressively mature and become activated, which is accompanied by an increase in the expression of cell surface CD costimulatory molecules. These molecules provide a second signal for T-cell and B-cell activation, resulting in the induction of cellular and humoral immune responses.[46] As mature DCs express high levels of CD11c, CD40, and CD86, evaluating the expression of these molecules by flow cytometry can determine whether nanoparticles can induce maturation in immature BMDCs. As shown in Figure 6A-C, the expression of CD40 and CD86 was significantly higher in the HZ-1, HSZ-1, HZ-2, and HSZ-2 groups than that in the PBS, HBsAg, and Alum + HBsAg

https://doi.org/10.1021/acsami.3c16358
ACS Appl. Mater. Interfaces XXXX, XXX, XXX−XXX

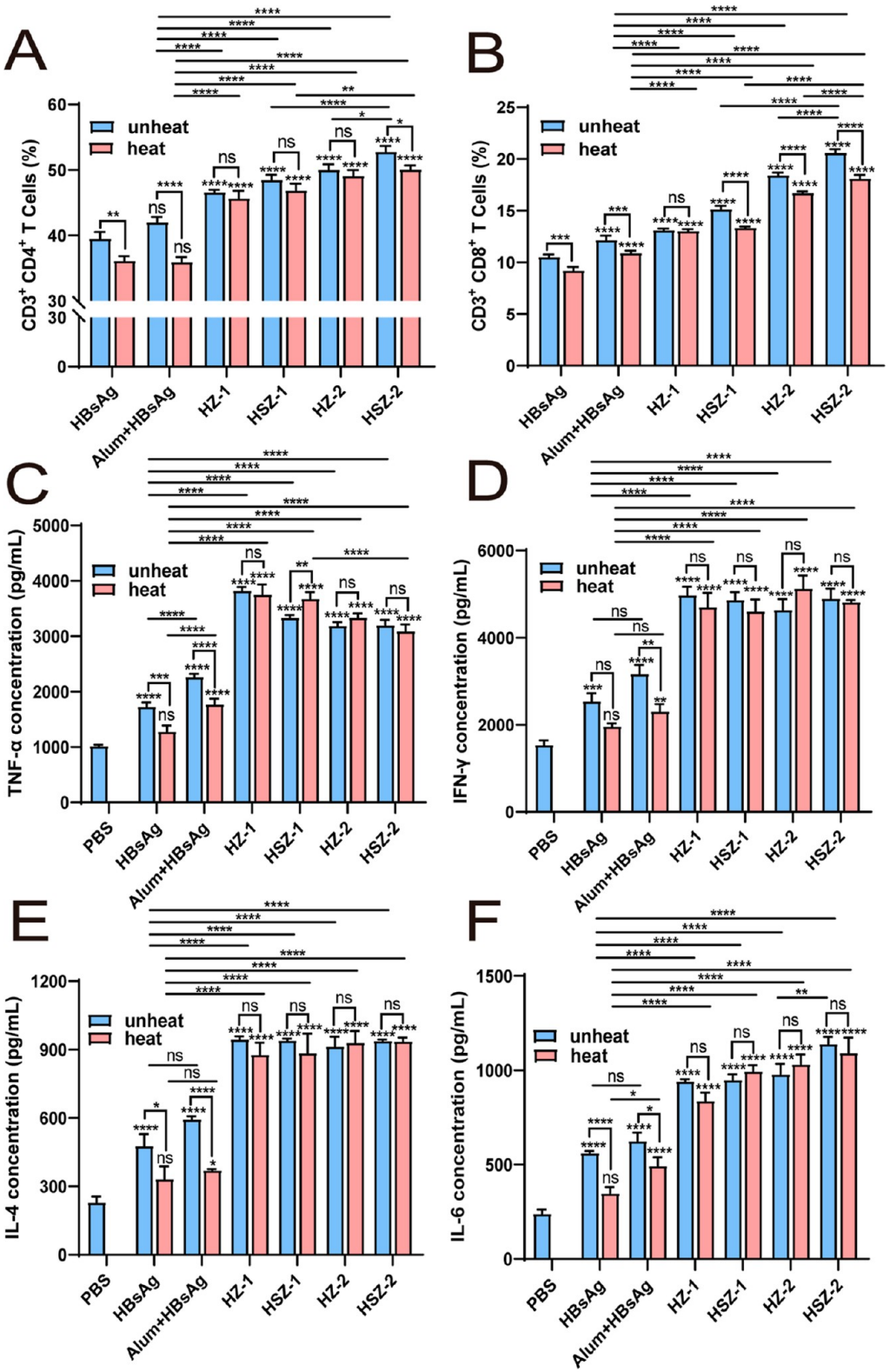

Figure 8. Changes in splenocyte population and cytokine levels in different immune groups. (A,B) $CD3^+CD4^+$ T and $CD3^+CD8^+$ T-cell populations in the splenocytes of immunized mice determined by flow cytometry. (C−F) Cytokines secreted by splenocytes after HBsAg restimulation in vitro, including TNF-α, IFN-γ, IL-4, and IL-6. *$p < 0.05$, **$p < 0.01$, ***$p < 0.001$, ****$p < 0.0001$; and ns: no significant difference.

groups and slightly higher in the HZ-2 and HSZ-2 groups than that in the HZ-1 and HSZ-1 groups. In addition, Alum + HBsAg did not increase the expression of CD40 and CD86 in BMDCs, which was similar to the results in the HBsAg group. This finding implies that SF-coated ZIF-8 more effectively promotes DC activation and maturation and induces immune responses stronger than those of traditional aluminum adjuvants.

https://doi.org/10.1021/acsami.3c16358
ACS Appl. Mater. Interfaces XXXX, XXX, XXX−XXX

The activation of APCs, such as macrophages and DCs, is usually accompanied by the secretion of proinflammatory cytokines, which is also a sign of activation of the immune response.[47] The secretion of TNF-α and IL-6 by Raw264.7 macrophages and IL-12p70 by BMDCs was evaluated using double antibody sandwich ELISA kits to determine whether cytokine secretion is increased during cell maturation. As shown in Figure 6D−F, HZ-1, HSZ-1, HZ-2, and HSZ-2 induced more IL-6, TNF-α, and IL-12p70 secretion than PBS, HBsAg, and Alum + HBsAg, a result consistent with the previous BMDCs maturation data. Furthermore, the levels in the HZ-2 and HSZ-2 groups were slightly higher than those in the HZ-1 and HSZ-1 groups and appeared to be the highest in the HSZ-2 group. This result implies that the nanoparticles prepared by the one-step shake method were superior to those prepared by the one-pot shake method. In conclusion, encapsulating HBsAg in SF-coated ZIF-8 helps promote the activation of BMDCs and the upregulation of cell surface CD costimulatory molecules and cytokines, which facilitate antigen delivery and induce a robust immune response in vivo.

HZ and HSZ Induce a Strong Immune Response. Currently, a majority of vaccines are extremely sensitive to temperature changes, necessitating the use of reliable cold chain storage and delivery systems to maintain consistent immunogenicity. To evaluate the adjuvant and protective effects of ZIF-8 and SF on HBsAg, the nanoparticles were stored at 25 °C for 14 days to study whether they could maintain their immunogenicity. To determine their produced immune response, mice were immunized with PBS (control), HBsAg, Alum + HBsAg, HZ-1, HSZ-1, HZ-2, HSZ-2, HBsAg (heat), Alum + HBsAg (heat), HZ-1 (heat), HSZ-1 (heat), HZ-2 (heat), and HSZ-2 (heat) by intramuscular injection. The ability of the animals to produce high quantities of antigen-specific antibodies is important in vaccine development when assessing the effect of a vaccine on the level of humoral immunity. As shown in Figure 7A, the specific IgG antibody titer increased in all groups with an increasing number of immunizations, and HZ and HSZ induced higher antibody levels than HBsAg and Alum + HBsAg from day 14. As shown in Figure 7B, the specific IgG titers in the HZ-1, HSZ-1, HZ-2, and HSZ-2 groups were significantly higher than those of the HBsAg and Alum + HBsAg groups at 35 days postimmunization, with the HSZ-2 group appearing to have the highest specific IgG titer. Notably, the specific IgG titers in the HZ-1, HSZ-1, HZ-2, and HSZ-2 groups were not significantly different before and after heat treatment, but significant differences were observed in the HBsAg and Alum + HBsAg groups. However, the heat-treated HSZ-2 group displayed antibody titers significantly higher than those of the HZ-2 group, which may be because the SF formed a more effective protective reservoir that resulted in a better slow release effect and more potent humoral immunity. After storage at 25 °C for 14 days, SF-coated ZIF-8 maintained the structural integrity of HBsAg without degradation and induced a significant immunological response, which was consistent with the results of the in vitro thermal stability studies. This protective and thermally stable composite may have promising applications in the future.

IgG antibodies are categorized into subtypes, with IgG2a being a marker of the T-helper 1 (Th1) immune response and IgG1 being a marker of the T-helper 2 (Th2) immune response.[48] As shown in Figure 7C,D, there was no difference in IgG1 and IgG2a levels in the HZ-1, HSZ-1, HZ-2, and HSZ-2 groups before and after heat treatment, but these were significantly higher than those in the HBsAg and Alum + HBsAg groups, indicating that heat treatment did not affect the humoral immunity of the vaccine. The IgG2a/IgG1 ratio indicates the tendency of the immune response and allows analysis of the extents of the cellular and humoral immune responses.[49] As shown in Figure 7E, HSZ-2 induced the highest IgG2a/IgG1 ratio, indicating that these nanoparticles induced a robust Th1-biased immune response with a cellular immune-enhancing effect and that the nanoparticles prepared by the one-step shake method were superior to those prepared by the one-pot shake method. In contrast, Alum + HBsAg may tend to produce IgG1 and was not better at boosting cellular immunity, which may be related to their own nature.

Splenocyte proliferation is another method used to assess the efficacy of vaccine immunity. Effector lymphocytes are rapidly activated to mount an immune response, and immune memory cells can proliferate rapidly upon restimulation with the same antigen in vitro.[50] As shown in Figure 7F, the splenocyte proliferation index in the HZ-1, HSZ-1, HZ-2, and HSZ-2 groups before and after heat treatment was significantly higher than those in the PBS, HBsAg, and Alum + HBsAg groups. The above results suggest that these nanoparticles can still produce a positive immunological memory effect even after heat treatment. The splenocyte proliferation index in the HZ-2 and HSZ-2 groups was significantly higher than those in the HZ-1 and HSZ-1 groups before and after heat treatment, demonstrating that once again, the nanoparticles prepared by the one-step shake method were superior to those produced by the one-pot shake method.

CD3 is a surface marker of mature T lymphocytes. $CD4^+$ T and $CD8^+$ T lymphocytes are critical components of the adaptive immune response, and their activation directly determines the strength of the subsequent immune response.[51] The percentages of $CD3^+CD4^+$ T and $CD3^+CD8^+$ T cells in the HSZ-2 group were higher than those in the other groups before and after heat treatment, up to approximately 52.8 and 20.6%, respectively (Figures 8A,B and S6,7). In contrast, the HBsAg and Alum + HBsAg groups showed lower T-cell responses before and after heat treatment, which may be due to degradation or insufficient cellular uptake. This suggests that SF-coated ZIF-8 not only promotes cellular and humoral immune responses but also enhances antigenic heat resistance. Then, the levels of cytokines secreted by the splenic lymphocytes of these immunized mice were measured. Th1-type cytokines, such as IL-2, IL-12, TNF-α and IFN-γ, can activate $CD8^+$ T cells, mediate CTLs killing, and regulate the cellular immune response. Th2-type cytokines, such as IL-4, IL-5, IL-6, and IL-10, can help B cells mature and regulate the humoral immune response.[52] As shown in Figure 8C−F, the levels of TNF-α, IFN-γ, IL-4, and IL-6 in the HZ-1, HSZ-1, HZ-2, and HSZ-2 groups were significantly higher than those in the PBS, HBsAg, and Alum + HBsAg groups, and there was no significant difference before and after heat treatment. However, the HBsAg and Alum + HBsAg groups had different degrees of difference before and after heat treatment. The results showed that SF-coated ZIF-8 enhanced Th1-type and Th2-type immune responses in vivo. In addition, Alum + HBsAg showed an effective humoral immune response capacity in vivo (Figure 7B). This result was not caused by cytokines (IL-4 and IL-6) produced by splenocytes and may be due to efficient antigen delivery and the formation of an antigen reservoir, which is consistent with previous reports in

https://doi.org/10.1021/acsami.3c16358
ACS Appl. Mater. Interfaces XXXX, XXX, XXX−XXX

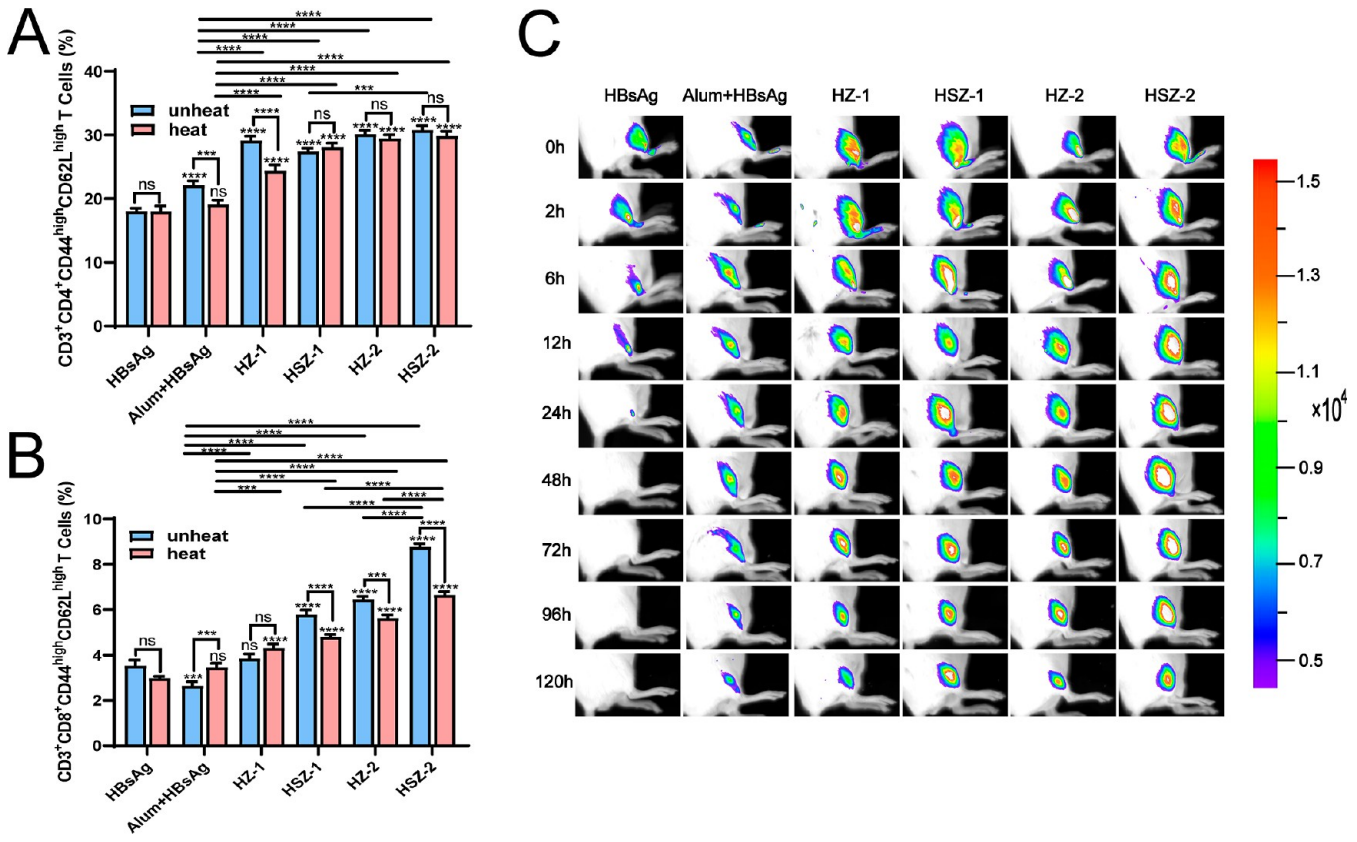

Figure 9. HZ and HSZ promote the production of $CD4^+$ and $CD8^+$ memory T cells and the formation of antigenic reservoirs. (A) Levels of T_{CM} in $CD4^+$ T cells ($CD3^+CD4^+CD44^{hi}CD62L^{hi}$) and (B) T_{CM} in $CD8^+$ T cells ($CD3^+CD8^+CD44^{hi}CD62L^{hi}$) were measured by flow cytometry. (C) Small animal fluorescence imaging system was used to observe the formation of antigen reservoirs at the injection sites in different immunological groups. *$p < 0.05$, **$p < 0.01$, ***$p < 0.001$, ****$p < 0.0001$; and ns: no significant difference.

the literature.[53,54] At the same time, the levels of IL-2, IL-12, and IL-5 in the HZ-1, HSZ-1, HZ-2, and HSZ-2 groups were significantly higher than those in the PBS, HBsAg, and Alum + HBsAg groups (Figure S8A−C). IL-2 and IL-12 regulate the differentiation of T-helper type 0 cells and promote their polarization into Th1 cells, thereby inducing a high level of a cellular immune response. IL-10 is an anti-inflammatory and immunosuppressive factor that affects the function of macrophages, monocytes, and DCs by inhibiting the expression of costimulatory molecules, proinflammatory factors, and chemokines.[55] The highest level of IL-10 expression was found in the Alum + HBsAg group (Figure S8D), while the proliferation of Th2 cells and secretion of associated cytokines suppressed Th1-type immune responses, which may explain the low level of cellular immunity produced by the aluminum adjuvant. In conclusion, SF-coated ZIF-8 not only enhanced the thermostability of the nanoparticles but also triggered strong humoral and cellular immunity, providing a theoretical basis for the storage and transport of the vaccine at RT.

HZ and HSZ Enhance Memory T-Cell Responses. One of the main aims of vaccination is to provide immunological memory, which allows the immune system to respond more quickly and efficiently when the body is exposed to the same pathogen for a second time after vaccination against a particular pathogen. For example, protection from HBV, which has an incubation period of 6 weeks to 6 months, typically results after vaccination and remains even after re-exposure to the virus after a long period of time, when the level of vaccine-induced antibodies has declined.[56] Therefore, the activation of memory T cells is critical for long-term HBV protection. The levels of $CD4^+$ central memory T cells (T_{CM}) and $CD8^+$ T_{CM} were significantly higher in the HZ-1, HSZ-1, HZ-2, and HSZ-2 groups than that in the HBsAg and Alum + HBsAg groups, and the results after heat treatment were the same (Figures 9A,B and S9, S10). Furthermore, the highest T_{CM} levels were observed in both $CD4^+$ (30.81%) and $CD8^+$ (8.78%) T cells in the HSZ-2 group, suggesting that the nanoparticles prepared by the one-step shake method were superior to those prepared by the one-pot shake method. In summary, these findings show that SF-coated ZIF-8 increases memory T-cell responses and can efficiently and rapidly initiate an immune response when the same antigen reappears to protect the body against reinfection.

HSZ Promotes the Formation of an Antigen Reservoir. Effective vaccination can lead to the creation of an antigen reservoir at the injection site, which is essential for eliciting a strong immune reaction. Therefore, the residence time of different nanoparticles was determined by using a small animal fluorescence imaging system. The fluorescence area in the HBsAg group was considerably reduced after 6 h, indicating that free HBsAg diffused more rapidly into the organism after injection. The fluorescence area in the Alum + HBsAg group was significantly diminished after 96 h, indicating that the aluminum adjuvant could form a gel at the injection site, which results in the slow release of the antigen. Intense fluorescence was still detected in the HZ-1, HSZ-1, HZ-2, and HSZ-2 groups after 120 h (Figure 9C). Over time, the fluorescence intensity and area in each group

https://doi.org/10.1021/acsami.3c16358
ACS Appl. Mater. Interfaces XXXX, XXX, XXX−XXX

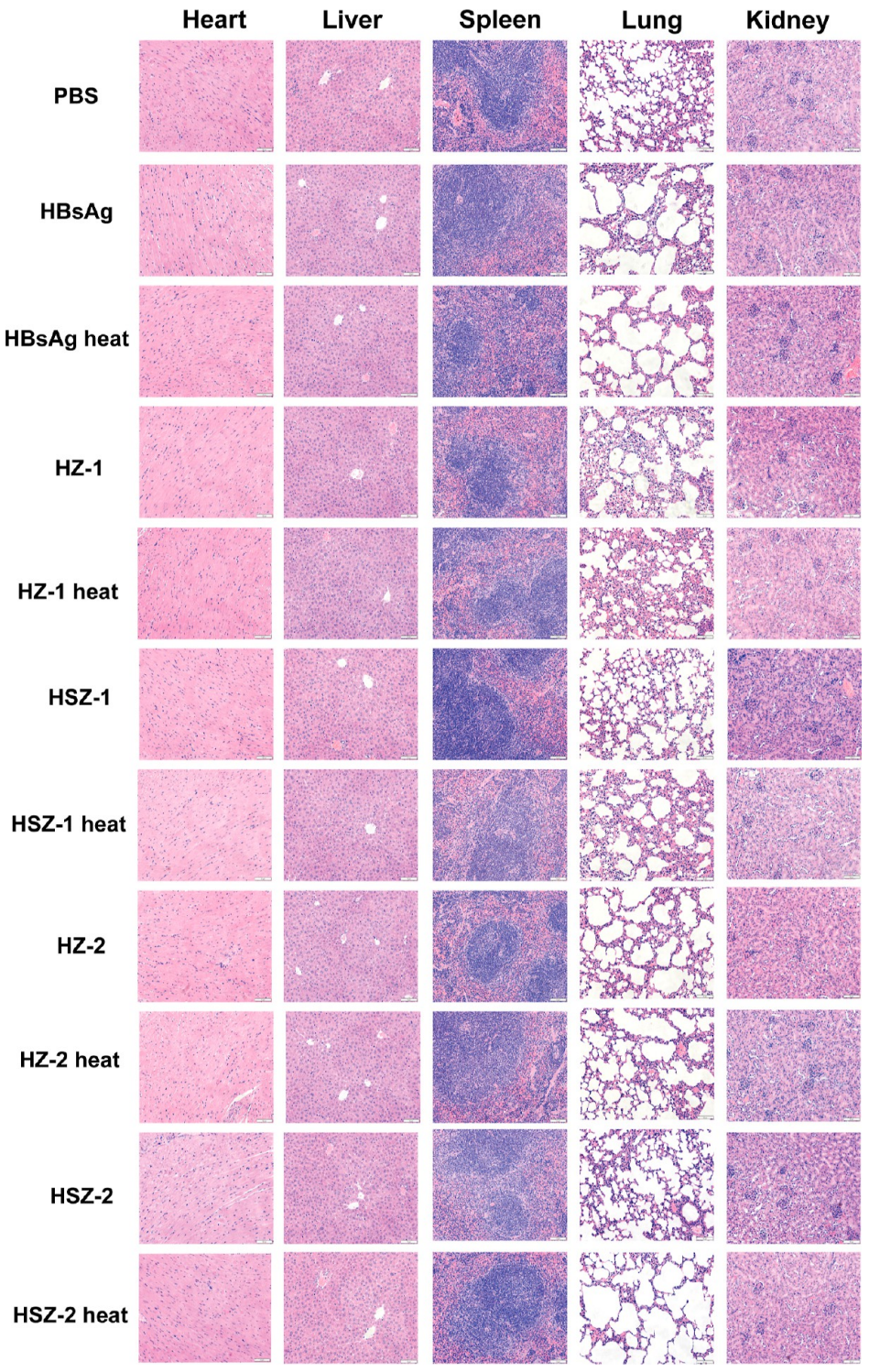

Figure 10. Histopathological studies of vital organs from different immunized mice. HE staining was performed for histopathological evaluations of the heart, liver, spleen, lung, and kidney in immunized mice.

progressively decreased. Notably, the fluorescence in the HSZ-1 and HSZ-2 groups was significantly higher than that in the HZ-1 and HZ-2 groups, indicating that modification with SF could further prolong the antigen presence. Furthermore, the data clearly show that the fluorescence in the HSZ-2 group was still the strongest after 120 h, again indicating that the one-step shake method is better than the one-pot shake method. The fluorescence area increased from 6 to 12 h, probably because HBsAg was encapsulated by ZIF-8 and SF, which masked some of the fluorescence signal, while after some time, HBsAg was released from the carrier, resulting in an increase in fluorescence intensity. These results suggest that SF-coated ZIF-8 can lead to the creation of an antigen reservoir, extend the antigen residence time, increase the antigen utilization rate, elicit a potent immune response through gradual release, and improve the vaccine efficacy.

Biodistribution of HSZ. In general, there are four mechanisms that nanomedicines can be broken down and

https://doi.org/10.1021/acsami.3c16358
ACS Appl. Mater. Interfaces XXXX, XXX, XXX−XXX

removed from the body, including excretion through the hepatobiliary and renal systems, biodegradation and utilization in the liver, accumulation in the mononuclear phagocytosis system, and gradual degradation in the body followed by excretion.[57] Zinc is one of the most essential trace elements in the human body, with approximately 60% of zinc is stored in skeletal muscle, 30% in bone, and 5% in the liver and skin.[58] Due to differences in the way vaccine immunization is considered, the distribution of zinc in major organs (heart, liver, spleen, lung, kidney, and muscle) of mice injected intramuscularly and tail vein with HSZ was studied by ICP-MS. After 5 days of intramuscular injection, zinc levels in kidney and heart are elevated, indicating that a small amount of zinc has been metabolized (Figure S11A). Zinc levels in the liver and kidney were significantly increased 2 days after tail vein injection of HSZ (Figure S11B). After injection, HSZ is primarily excreted through the hepatobiliary and renal systems.

Biocompatibility Evaluation. In vivo and in vitro safety is critical for vaccines. In this study, the biocompatibility of SF-coated ZIF-8 was assessed by determining the body weight, viscera indices, and pathological changes in vital organs. All mice showed an increasing trend in body weight (Figure S12). The viscera index is widely used in toxicological safety evaluations, and the organ/body weight ratio is relatively constant under normal conditions.[59] There were no significant differences in the heart, lung, spleen, liver, and kidney indices of the immunized mice in any of the groups compared to the PBS group (Figure S13). Moreover, in contrast to the PBS group, the immunized mice did not show any significant pathological changes or inflammatory reactions in their heart, liver, spleen, lung, or kidney (Figure 10). The ICP-MS results show that the nanoparticles are excreted through the liver and kidneys. To confirm the safety of the nanoparticles, the organ function of immunized mice was evaluated using biochemical indices. The results showed that all of the indices were within the normal range, indicating that there was no effect on the biochemical indices of the mice after immunization (Table S1). This further substantiates the excellent biocompatibility of the nanoparticles. Taken together, these results indicate that the nanoparticles are biocompatible and do not cause adverse conditions in mice.

Comparative Analysis. Compared to freeze-drying and genetic engineering to improve the thermal stability of influenza vaccine,[27] human immunodeficiency virus type 1 vaccine,[60] and classical swine fever vaccine,[61] HSZ does not require a complex preparation process, can be performed in a short time, and is cost-effective (Table S2). Long-term stability is also a key factor in the use of vaccines, and this part of the study is the focus of our subsequent research. In addition, this study was conducted on a small scale in the laboratory, and the next study will focus on whether it can be efficiently produced on a large scale. More importantly, SF-coated ZIF-8 is expected to improve the immunogenicity and thermal stability of various subunit vaccines and is also expected to be used to protect the stability of enzymes, drugs, and live viruses. In conclusion, SF-coated ZIF-8 is not only easy to prepare but also improves the thermal stability and immunogenicity of HBsAg, which is expected to be applied to a variety of macromolecules and expand the application of MOFs in biomedical fields.

CONCLUSIONS

In this study, we prepared HZ by encapsulating HBsAg in ZIF-8 using a one-pot shake method and a one-step shake method in an aqueous solution. The SF coatings then self-assembled on the modified HZ surface by the hydrophobic interaction to form HSZ. The preparation methods are simple, environmentally friendly, and inexpensive, and HSZ showed good biocompatibility both in vivo and in vitro. The appropriately sized HSZ facilitates the internalization of HBsAg into APCs and promotes the maturation of DCs and lysosomal escape of HBsAg, which is beneficial for vaccine delivery. HSZ formed an antigen reservoir at the injection site and significantly promoted humoral and cellular immunity, including increased HBsAg-specific IgG antibody production, induction of $CD4^+$ T and $CD8^+$ T-cell responses, enhanced cytokine secretion (including TNF-α, IFN-γ, IL-2, IL-4, IL-5, IL-6, IL-10, and IL-12) by splenocytes, and production of memory T-cells. In addition, HSZ maintained antibody levels comparable to the control group after 14 days of storage at 25 °C. Overall, SF-coated ZIF-8 is expected to be produced as a thermostable vaccine with enhanced immune responses, which could pave the way for the development of next-generation novel vaccines with high performance and independence from cold chain storage and transport.

ASSOCIATED CONTENT

Supporting Information

The Supporting Information is available free of charge at https://pubs.acs.org/doi/10.1021/acsami.3c16358.

FT-IR spectra of pure SF, quantification of HBsAg encapsulated in HZ and HSZ, photograph hemolysis assays, solution stability, flow cytometry graphs of $CD4^+/CD8^+$ T lymphocytes and $CD4^+/CD8^+$ T_{CM} in the spleen, biodistribution of HSZ, mice body weight changes during immunization, cytokines secreted by splenocytes, visceral indices, and serum biochemical indices in mice at the end of immunization (PDF)

AUTHOR INFORMATION

Corresponding Authors

Qianxue Li − *Changchun Veterinary Research Institute, Chinese Academy of Agricultural Sciences, Changchun 130012, China*; Email: lqxue@hotmail.com

Jiali Zhang − *College of Veterinary Medicine, Jilin Agricultural University, Changchun 130118, China*; Email: zhangjialijlau@163.com

Jianxu Zhang − *Changchun Veterinary Research Institute, Chinese Academy of Agricultural Sciences, Changchun 130012, China*; Email: longde.guxiang@163.com

Authors

Jiabin Zhang − *College of Veterinary Medicine, Jilin Agricultural University, Changchun 130118, China; Changchun Veterinary Research Institute, Chinese Academy of Agricultural Sciences, Changchun 130012, China*; orcid.org/0009-0005-3775-2868

Kai Wang − *Changchun Veterinary Research Institute, Chinese Academy of Agricultural Sciences, Changchun 130012, China*

Shiyao Xu − *College of Life Sciences, Tonghua Normal University, Tonghua 134002, China*

Linlin Chen − *College of Veterinary Medicine, Jilin Agricultural University, Changchun 130118, China*

https://doi.org/10.1021/acsami.3c16358
ACS Appl. Mater. Interfaces XXXX, XXX, XXX−XXX

Haiquan Gu − *Changchun Veterinary Research Institute, Chinese Academy of Agricultural Sciences, Changchun 130012, China*
Yujie Yang − *Changchun Veterinary Research Institute, Chinese Academy of Agricultural Sciences, Changchun 130012, China*
Qi Zhao − *Changchun Veterinary Research Institute, Chinese Academy of Agricultural Sciences, Changchun 130012, China*
Yurou Huo − *Changchun Veterinary Research Institute, Chinese Academy of Agricultural Sciences, Changchun 130012, China*
Bo Li − *College of Veterinary Medicine, Jilin Agricultural University, Changchun 130118, China*
Yufei Wang − *College of Veterinary Medicine, Jilin Agricultural University, Changchun 130118, China*
Yubiao Xie − *Changchun Veterinary Research Institute, Chinese Academy of Agricultural Sciences, Changchun 130012, China*
Nan Li − *Changchun Veterinary Research Institute, Chinese Academy of Agricultural Sciences, Changchun 130012, China*

Complete contact information is available at: https://pubs.acs.org/10.1021/acsami.3c16358

Author Contributions

[‖]J.Z. and K.W. contributed equally. All authors have given approval to the final version of the manuscript.

Notes

The authors declare no competing financial interest.

■ ACKNOWLEDGMENTS

This work was financially supported by the National Natural Science Foundation of China (31902224 and 32001004).

■ ABBREVIATIONS

MOFs, metal−organic frameworks; ZIF-8, zeolitic imidazolate framework-8; SF, silk fibroin; HBV, hepatitis B virus; COVID-19, corona virus disease 2019; HBsAg, hepatitis B surface antigen; HZ, HBsAg@ZIF-8; HSZ, HBsAg/SF@ZIF-8; APCs, antigen-presenting cells; BMDCs, bone marrow-derived DCs; GM-CSF, granulocyte-macrophage colony-stimulating factor; Th1, T-helper 1; Th2, T-helper 2; PEG, polyethylene glycol; MHC I, major histocompatibility complex I; MHC II, major histocompatibility complex II; CTLs, cytotoxic T-lymphocytes; RT, room temperature

■ REFERENCES

(1) Jeng, W. J.; Papatheodoridis, G. V.; Lok, A. S. F.; Hepatitis, B. Hepatitis B. *Lancet* **2023**, *401* (10381), 1039−1052.
(2) Terrault, N. A.; Lok, A. S. F.; McMahon, B. J.; Chang, K. M.; Hwang, J. P.; Jonas, M. M.; Brown, R. S. Jr.; Bzowej, N. H.; Wong, J. B. Update on Prevention, Diagnosis, and Treatment of Chronic Hepatitis B: AASLD 2018 Hepatitis B Guidance. *Clin. Liver Dis.* **2018**, *12* (1), 33−34.
(3) Brody, H.; Hepatitis, B. Hepatitis B. *Nature* **2022**, *603* (7903), S45.
(4) Doi, H.; Kanto, T. Factors influencing the durability of hepatitis B vaccine responses. *Vaccine* **2021**, *39* (36), 5224−5230.
(5) Liaw, Y. F.; Kao, J. H.; Piratvisuth, T.; Chan, H. L.; Chien, R. N.; Liu, C. J.; Gane, E.; Locarnini, S.; Lim, S. G.; Han, K. H.; Amarapurkar, D.; Cooksley, G.; Jafri, W.; Mohamed, R.; Hou, J. L.; Chuang, W. L.; Lesmana, L. A.; Sollano, J. D.; Suh, D. J.; Omata, M. Asian-Pacific consensus statement on the management of chronic hepatitis B: a 2012 update. *Hepatol. Int.* **2012**, *6* (3), 531−561.
(6) Locarnini, S.; Hatzakis, A.; Chen, D. S.; Lok, A. Strategies to control hepatitis B: Public policy, epidemiology, vaccine and drugs. *J. Hepatol.* **2015**, *62* (1), S76−S86.
(7) Ćirović, A.; Ćirović, A.; Nikolić, D.; Ivanovski, A.; Ivanovski, P. The adjuvant aluminum fate - Metabolic tale based on the basics of chemistry and biochemistry. *J. Trace Elem. Med. Biol.* **2021**, *68*, 126822.
(8) Badran, G.; Angrand, L.; Masson, J. D.; Crépeaux, G.; David, M. O. Physico-chemical properties of aluminum adjuvants in vaccines: Implications for toxicological evaluation. *Vaccine* **2022**, *40* (33), 4881−4888.
(9) HogenEsch, H.; O'Hagan, D. T.; Fox, C. B. Optimizing the utilization of aluminum adjuvants in vaccines: you might just get what you want. *npj Vaccines* **2018**, *3*, 51.
(10) Kundi, M. New hepatitis B vaccine formulated with an improved adjuvant system. *Expert Rev. Vaccines* **2007**, *6* (2), 133−140.
(11) Chen, C. H.; Lee, C. M.; Wang, J. H.; Tung, H. D.; Hung, C. H.; Lu, S. N. Correlation of quantitative assay of hepatitis B surface antigen and HBV DNA levels in asymptomatic hepatitis B virus carriers. *Eur. J. Gastroenterol. Hepatol.* **2004**, *16* (11), 1213−1218.
(12) Chen, X.; Fernando, G. J.; Crichton, M. L.; Flaim, C.; Yukiko, S. R.; Fairmaid, E. J.; Corbett, H. J.; Primiero, C. A.; Ansaldo, A. B.; Frazer, I. H.; Brown, L. E.; Kendall, M. A. Improving the reach of vaccines to low-resource regions, with a needle-free vaccine delivery device and long-term thermostabilization. *J. Controlled Release* **2011**, *152* (3), 349−355.
(13) Schlehuber, L. D.; McFadyen, I. J.; Shu, Y.; Carignan, J.; Duprex, W. P.; Forsyth, W. R.; Ho, J. H.; Kitsos, C. M.; Lee, G. Y.; Levinson, D. A.; Lucier, S. C.; Moore, C. B.; Nguyen, N. T.; Ramos, J.; Weinstock, B. A.; Zhang, J.; Monagle, J. A.; Gardner, C. R.; Alvarez, J. C. Towards ambient temperature-stable vaccines: the identification of thermally stabilizing liquid formulations for measles virus using an innovative high-throughput infectivity assay. *Vaccine* **2011**, *29* (31), 5031−5039.
(14) Lydon, P.; Raubenheimer, T.; Arnot-Krüger, M.; Zaffran, M. Outsourcing vaccine logistics to the private sector: The evidence and lessons learned from the Western Cape Province in South-Africa. *Vaccine* **2015**, *33* (29), 3429−3434.
(15) Wang, L.; Li, J.; Chen, H.; Li, F.; Armstrong, G. L.; Nelson, C.; Ze, W.; Shapiro, C. N. Hepatitis B vaccination of newborn infants in rural China: evaluation of a village-based, out-of-cold-chain delivery strategy. *Bull. W. H. O.* **2007**, *85* (09), 688−694.
(16) Hipgrave, D. B.; Maynard, J. E.; Van, N. T.; Long, H. T.; Tran, T. N.; Nga, N. T.; Dat, D. T.; Huong, V. M.; Biggs, B. A. Immunogenicity of a locally produced hepatitis B vaccine with the birth dose stored outside the cold chain in rural Vietnam. *Am. J. Trop. Med. Hyg.* **2006**, *74* (2), 255.
(17) Breakwell, L.; Anga, J.; Dadari, I.; Sadr-Azodi, N.; Ogaoga, D.; Patel, M. Evaluation of storing hepatitis B vaccine outside the cold chain in the Solomon Islands: Identifying opportunities and barriers to implementation. *Vaccine* **2017**, *35* (21), 2770−2774.
(18) Kolwaite, A. R.; Xeuatvongsa, A.; Ramirez-Gonzalez, A.; Wannemuehler, K.; Vongxay, V.; Vilayvone, V.; Hennessey, K.; Patel, M. K. Hepatitis B vaccine stored outside the cold chain setting: a pilot study in rural Lao PDR. *Vaccine* **2016**, *34* (28), 3324.
(19) Pelliccia, M.; Andreozzi, P.; Paulose, J.; D'Alicarnasso, M.; Cagno, V.; Donalisio, M.; Civra, A.; Broeckel, R. M.; Haese, N.; Jacob Silva, P.; Carney, R. P.; Marjomäki, V.; Streblow, D. N.; Lembo, D.; Stellacci, F.; Vitelli, V.; Krol, S. Additives for vaccine storage to improve thermal stability of adenoviruses from hours to months. *Nat. Commun.* **2016**, *7*, 13520.
(20) Yamamoto, S.; Yamamoto, T. Historical review of BCG vaccine in Japan. *Jpn. J. Infect. Dis.* **2007**, *60*, 331−336.
(21) Shokri, S.; Shahkarami, M. K.; Shafyi, A.; Mohammadi, A.; Esna-Ashari, F.; Hamta, A. Evaluation of the thermal stability of live-attenuated Rubella vaccine (Takahashi strain) formulated and lyophilized in different stabilizers. *J. Virol. Methods* **2019**, *264*, 18−22.
(22) Mateo, R.; Luna, E.; Rincón, V.; Mateu, M. G. Engineering Viable Foot-and-Mouth Disease Viruses with Increased Thermo-

stability as a Step in the Development of Improved Vaccines. *J. Virol.* **2008**, *82* (24), 12232−12240.
(23) Shang, Y.; Li, L.; Zhang, T.; Luo, Q.; Yu, Q.; Zeng, Z.; Li, L.; Jia, M.; Tang, G.; Fan, S.; Lu, Q.; Zhang, W.; Xue, Y.; Wang, H.; Liu, W.; Wang, H.; Zhang, R.; Ding, C.; Shao, H.; Wen, G. Quantitative regulation of the thermal stability of enveloped virus vaccines by surface charge engineering to prevent the self-aggregation of attachment glycoproteins. *PLoS Pathog.* **2022**, *18* (6), No. e1010564.
(24) Westfall, J.; Yates, J. L.; Van Slyke, G.; Ehrbar, D.; Measey, T.; Straube, R.; Donini, O.; Mantis, N. J. Thermal stability and epitope integrity of a lyophilized ricin toxin subunit vaccine. *Vaccine* **2018**, *36* (40), 5967−5976.
(25) Kunda, N. K.; Peabody, J.; Zhai, L.; Price, D. N.; Chackerian, B.; Tumban, E.; Muttil, P. Evaluation of the thermal stability and the protective efficacy of spray-dried HPV vaccine, Gardasil 9. *Hum. Vaccines Immunother.* **2019**, *15* (7−8), 1995−2002.
(26) Lyu, F.; Zhao, Y. H.; Lu, Y.; Zuo, X. X.; Deng, B. H.; Zeng, M. Q.; Wang, J. N.; Olaniran, A.; Hou, J.; Khoza, T. Vacuum Foam Drying Method Improved the Thermal Stability and Long-Term Shelf Life of a Live Attenuated Newcastle Disease Virus Vaccine. *AAPS PharmSciTech* **2022**, *23* (8), 291.
(27) Ingrole, R. S. J.; Tao, W.; Joshi, G.; Gill, H. S. M2e conjugated gold nanoparticle influenza vaccine displays thermal stability at elevated temperatures and confers protection to ferrets. *Vaccine* **2021**, *39* (34), 4800−4809.
(28) Peng, F.; Xiang, Y.; Wang, H.; Hu, Y.; Zhou, R.; Hu, Y. Biomimetic Assembly of Spore@ZIF-8 Microspheres for Vaccination. *Small* **2022**, *18* (38), No. e2204011.
(29) Tzeng, S. Y.; Guarecuco, R.; McHugh, K. J.; Rose, S.; Rosenberg, E. M.; Zeng, Y.; Langer, R.; Jaklenec, A. Thermostabilization of inactivated polio vaccine in PLGA-based microspheres for pulsatile release. *J. Controlled Release* **2016**, *233*, 101−113.
(30) Teng, Z.; Hou, F.; Bai, M.; Li, J.; Wang, J.; Wu, J.; Ru, J.; Ren, M.; Sun, S.; Guo, H. Bio-mineralization of virus-like particles by metal-organic framework nanoparticles enhances the thermostability and immune responses of the vaccines. *J. Mater. Chem. B* **2022**, *10* (15), 2853−2864.
(31) Voigt, E. A.; Gerhardt, A.; Hanson, D.; Jennewein, M. F.; Battisti, P.; Reed, S.; Singh, J.; Mohamath, R.; Bakken, J.; Beaver, S.; Press, C.; Soon-Shiong, P.; Paddon, C. J.; Fox, C. B.; Casper, C. A self-amplifying RNA vaccine against COVID-19 with long-term room-temperature stability. *npj Vaccines* **2022**, *7* (1), 136.
(32) Wang, Z.; Cui, K.; Costabel, U.; Zhang, X. Nanotechnology-facilitated vaccine development during the coronavirus disease 2019 (COVID-19) pandemic. *Exploration* **2022**, *2* (5), 20210082.
(33) Yang, Y.; Chen, Q.; Wu, J. P.; Kirk, T. B.; Xu, J.; Liu, Z.; Xue, W. Reduction-Responsive Codelivery System Based on a Metal-Organic Framework for Eliciting Potent Cellular Immune Response. *ACS Appl. Mater. Interfaces* **2018**, *10* (15), 12463−12473.
(34) Li, Z.; Liu, J.; Feng, L.; Pan, Y.; Tang, J.; Li, H.; Cheng, G.; Li, Z.; Shi, J.; Xu, Y.; Liu, W. Monolithic MOF-Based Metal-Insulator-Metal Resonator for Filtering and Sensing. *Nano Lett.* **2023**, *23* (2), 637−644.
(35) Zhang, G.; Fu, X.; Sun, H.; Zhang, P.; Zhai, S.; Hao, J.; Cui, J.; Hu, M. Poly(ethylene glycol)-Mediated Assembly of Vaccine Particles to Improve Stability and Immunogenicity. *ACS Appl. Mater. Interfaces* **2021**, *13* (12), 13978−13989.
(36) Vodyashkin, A. A.; Sergorodceva, A. V.; Kezimana, P.; Stanishevskiy, Y. M. Metal-Organic Framework (MOF)-A Universal Material for Biomedicine. *Int. J. Mol. Sci.* **2023**, *24* (9), 7819.
(37) Yang, Y.; Chen, Q.; Wu, J. P.; Kirk, T. B.; Xu, J.; Liu, Z.; Xue, W. Reduction-Responsive Codelivery System Based on a Metal-Organic Framework for Eliciting Potent Cellular Immune Response. *ACS Appl. Mater. Interfaces* **2018**, *10* (15), 12463−12473.
(38) Liang, K.; Ricco, R.; Doherty, C. M.; Styles, M. J.; Bell, S.; Kirby, N.; Mudie, S.; Haylock, D.; Hill, A. J.; Doonan, C. J.; Falcaro, P. Biomimetic mineralization of metal-organic frameworks as protective coatings for biomacromolecules. *Nat. Commun.* **2015**, *6*, 7240.
(39) Luzuriaga, M. A.; Welch, R. P.; Dharmarwardana, M.; Benjamin, C. E.; Li, S.; Shahrivarkevishahi, A.; Popal, S.; Tuong, L. H.; Creswell, C. T.; Gassensmith, J. J. Enhanced Stability and Controlled Delivery of MOF-Encapsulated Vaccines and Their Immunogenic Response In Vivo. *ACS Appl. Mater. Interfaces* **2019**, *11* (10), 9740−9746.
(40) Nguyen, T. P.; Nguyen, Q. V.; Nguyen, V. H.; Le, T. H.; Huynh, V. Q. N.; Vo, D. V. N.; Trinh, Q. T.; Kim, S. Y.; Le, Q. V. Silk Fibroin-Based Biomaterials for Biomedical Applications: A Review. *Polymers* **2019**, *11* (12), 1933.
(41) Wang, X.; Wenk, E.; Hu, X.; Castro, G. R.; Meinel, L.; Wang, X.; Li, C.; Merkle, H.; Kaplan, D. L. Silk coatings on PLGA and alginate microspheres for protein delivery. *Biomaterials* **2007**, *28* (28), 4161−4169.
(42) Stinson, J. A.; Palmer, C. R.; Miller, D. P.; Li, A. B.; Lightner, K.; Jost, H.; Weldon, W. C.; Oberste, M. S.; Kluge, J. A.; Kosuda, K. M. Thin silk fibroin films as a dried format for temperature stabilization of inactivated polio vaccine. *Vaccine* **2020**, *38* (7), 1652−1660.
(43) Park, S.; Kim, S. I.; Choi, J. H.; Kim, S. E.; Choe, S. H.; Son, Y.; Kang, T. W.; Song, J. E.; Khang, G. Evaluation of Silk Fibroin/Gellan Gum Hydrogels with Controlled Molecular Weight through Silk Fibroin Hydrolysis for Tissue Engineering Application. *Molecules* **2023**, *28* (13), 5222.
(44) Liu, X.; Liu, Y.; Yang, X.; Lu, X.; Xu, X. N.; Zhang, J.; Chen, R. Potentiating the Immune Responses of HBsAg-VLP Vaccine Using a Polyphosphoester-Based Cationic Polymer Adjuvant. *ACS Appl. Mater. Interfaces* **2023**, *15* (42), 48871−48881.
(45) Dong, K.; Wang, Z.; Zhang, Y.; Ren, J.; Qu, X. Metal-Organic Framework-Based Nanoplatform for Intracellular Environment-Responsive Endo/Lysosomal Escape and Enhanced Cancer Therapy. *ACS Appl. Mater. Interfaces* **2018**, *10* (38), 31998−32005.
(46) Blom, R. A. M.; Amacker, M.; Moser, C.; van Dijk, R. M.; Bonetti, R.; Seydoux, E.; Hall, S. R. R.; von Garnier, C.; Blank, F. Virosome-bound antigen enhances DC-dependent specific CD4+ T cell stimulation, inducing a Th1 and Treg profile in vitro. *Nanomedicine* **2017**, *13* (5), 1725−1737.
(47) Eckshtain-Levi, M.; Batty, C. J.; Lifshits, L. M.; McCammitt, B.; Moore, K. M.; Amouzougan, E. A.; Stiepel, R. T.; Duggan, E.; Ross, T. M.; Bachelder, E. M.; Ainslie, K. M. Metal-Organic Coordination Polymer for Delivery of a Subunit Broadly Acting Influenza Vaccine. *ACS Appl. Mater. Interfaces* **2022**, *14* (25), 28548−28558.
(48) Gaikwad, S.; Pawar, Y.; Banerjee, S.; Kulkarni, S. Potential immunomodulatory effect of allelochemical juglone in mice vaccinated with BCG. *Toxicon* **2019**, *157*, 43−52.
(49) McCrudden, C. M.; Bennie, L.; Chambers, P.; Wilson, J.; Kerr, M.; Ziminska, M.; Douglas, H.; Kuhn, S.; Carroll, E.; O'Brien, G.; Buckley, N.; Dunne, N. J.; McCarthy, H. O. Peptide delivery of a multivalent mRNA SARS-CoV-2 vaccine. *J. Controlled Release* **2023**, *362*, 536−547.
(50) Cibulski, S.; Varela, A. P. M.; Teixeira, T. F.; Cancela, M. P.; Sesterheim, P.; Souza, D. O.; Roehe, P. M.; Silveira, F. Zika Virus Envelope Domain III Recombinant Protein Delivered With Saponin-Based Nanoadjuvant From Quillaja brasiliensis Enhances Anti-Zika Immune Responses, Including Neutralizing Antibodies and Splenocyte Proliferation. *Front. Immunol.* **2021**, *12*, 632714.
(51) Rincon-Restrepo, M.; Mayer, A.; Hauert, S.; Bonner, D. K.; Phelps, E. A.; Hubbell, J. A.; Swartz, M. A.; Hirosue, S. Vaccine nanocarriers: Coupling intracellular pathways and cellular biodistribution to control CD4 vs CD8 T cell responses. *Biomaterials* **2017**, *132*, 48−58.
(52) Kisuya, J.; Chemtai, A.; Raballah, E.; Keter, A.; Ouma, C. The diagnostic accuracy of Th1 (IFN-γ, TNF-α, and IL-2) and Th2 (IL-4, IL-6 and IL-10) cytokines response in AFB microscopy smear negative PTB- HIV co-infected patients. *Sci. Rep.* **2019**, *9* (1), 2966.
(53) Gupta, R. K. Aluminum compounds as vaccine adjuvants. *Adv. Drug Delivery Rev.* **1998**, *32* (3), 155−172.

https://doi.org/10.1021/acsami.3c16358
ACS Appl. Mater. Interfaces XXXX, XXX, XXX−XXX

(54) Lu, F.; Hogenesch, H. Kinetics of the inflammatory response following intramuscular injection of aluminum adjuvant. *Vaccine* **2013**, *31* (37), 3979−3986.
(55) Oleszycka, E.; McCluskey, S.; Sharp, F. A.; Muñoz-Wolf, N.; Hams, E.; Gorman, A. L.; Fallon, P. G.; Lavelle, E. C. The vaccine adjuvant alum promotes IL-10 production that suppresses Th1 responses. *Eur. J. Immunol.* **2018**, *48* (4), 705−715.
(56) Pollard, A. J.; Bijker, E. M. A guide to vaccinology: from basic principles to new developments. *Nat. Rev. Immunol.* **2021**, *21* (2), 83−100.
(57) Cao, M.; Chen, C. Bioavailability of nanomaterials: bridging the gap between nanostructures and their bioactivity. *Natl. Sci. Rev.* **2022**, *9* (10), nwac119.
(58) Kambe, T.; Tsuji, T.; Hashimoto, A.; Itsumura, N. The Physiological, Biochemical, and Molecular Roles of Zinc Transporters in Zinc Homeostasis and Metabolism. *Physiol. Rev.* **2015**, *95* (3), 749−784.
(59) Ding, J.; Gao, X.; Zhang, F.; Zhou, Y.; Li, S.; Lu, Y.; Liu, Q. Toxicological safety evaluation of Qiguiyin formula in rats at the treatment phase and recovery phase. *J. Ethnopharmacol.* **2021**, *279*, 114364.
(60) Aguado-Garcia, D.; Olvera, A.; Brander, C.; Sanchez-Merino, V.; Yuste, E. Evaluation of the Thermal Stability of a Vaccine Prototype Based on Virus-like Particle Formulated HIV-1 Envelope. *Vaccines* **2022**, *10* (4), 484.
(61) Zuo, X. X.; Zhao, Y. H.; Zhou, M. X.; Deng, B. H.; Hu, L. G.; Lv, F.; Lu, Y.; Hou, J. B. Live vaccine preserved at room temperature: Preparation and characterization of a freeze-dried classical swine fever virus vaccine. *Vaccine* **2020**, *38* (52), 8371−8378.

https://doi.org/10.1021/acsami.3c16358
ACS Appl. Mater. Interfaces XXXX, XXX, XXX−XXX